

RESEARCH

Open Access



# Chitosan based extruded nanofibrous bioscaffold for local delivery of mesenchymal stem cells to improve diabetic wound healing

Alyeh Abdollahi<sup>1</sup>, Hamid Reza Aghayan<sup>2</sup>, Zahra Mousivand<sup>3</sup>, Hamidreza Motasadizadeh<sup>4</sup>, Samane Maghsoudian<sup>5</sup>, Mohammadmohsen Abdorashidi<sup>6</sup>, Seyed Nasser Ostad<sup>7</sup>, Bagher Larijani<sup>8</sup>, Mohammad Raoufi<sup>9</sup> and Hamid Akbari Javar<sup>10\*</sup>

## Abstract

**Background** Mesenchymal stem cells (MSCs)-based treatment strategy has shown promise in bolstering the healing process of chronic wounds in diabetic patients, who are at risk of amputation and mortality. To overcome the drawbacks of suboptimal cell retention and diminished cell viability at the injury site, a novel nanofibrous biomaterial-based scaffold was developed by using a controlled extrusion of a polymeric solution to deliver the cells (human adipose-derived MSCs (ADMSCs) and placenta-derived MSCs (PLMSCs)) locally to the animal model of diabetic ulcers.

**Methods** The physicochemical and biological properties of the nano-bioscaffold were characterized in terms of microscopic images, FTIR spectroscopy, tensile testing, degradation and swelling tests, contact angle measurements, MTT assay, and cell attachment evaluation. To evaluate the therapeutic efficacy, a study using an excisional wound model was conducted on diabetic rats.

**Results** The SEM and AFM images of scaffolds revealed a network of uniform nanofibers with narrow diameters between 100-130 nm and surface roughness less than 5 nm, respectively. ADMSCs and PLMSCs had a typical spindle-shaped or fibroblast-like morphology when attached to the scaffold. Desired characteristics in terms of swelling, hydrophilicity, biodegradation rate, and biocompatibility were achieved with the CS70 formulation. The wound healing process was accelerated according to wound closure rate assay upon treatment with MSCs loaded scaffold resulting in increased re-epithelialization, neovascularization, and less inflammatory reaction. Our findings unequivocally demonstrated that the cell-loaded nano-bioscaffold exhibited more efficacy compared with its acellular counterpart. In summation, our study underscores the potential of this innovative cellular scaffold as a viable solution for enhancing the healing of diabetic ulcers.

**Conclusion** The utilization of MSCs in a nanofibrous biomaterial framework demonstrates significant promise, providing a novel avenue for advancing wound care and diabetic ulcer management.

**Keywords** Adipose tissue, Bioscaffold, Diabetic ulcers, Extrusion method, Nanofibrous, Mesenchymal stem cells, Placenta

\*Correspondence:

Hamid Akbari Javar

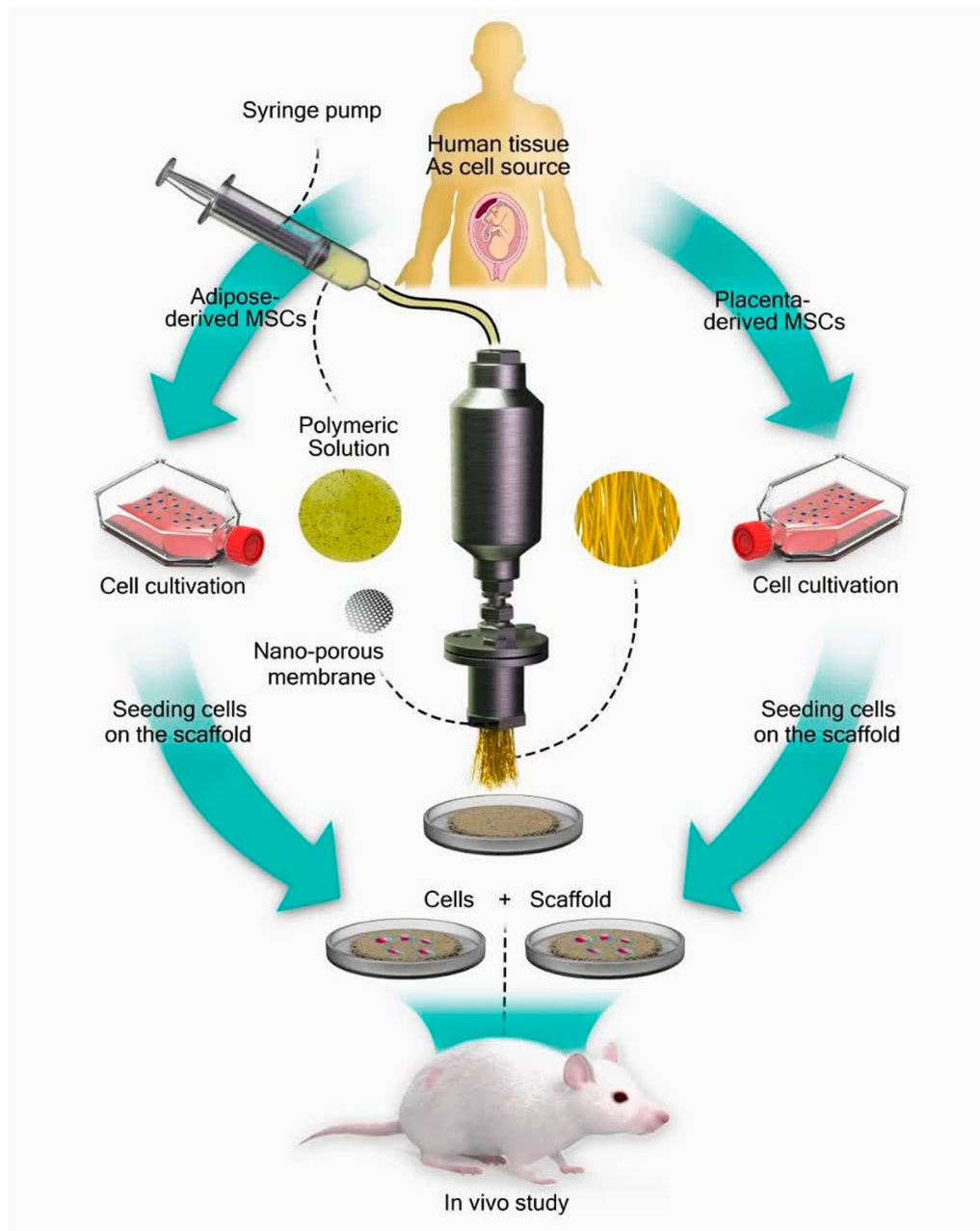
akbarijo@tums.ac.ir

Full list of author information is available at the end of the article



© The Author(s) 2024. **Open Access** This article is licensed under a Creative Commons Attribution-NonCommercial-NoDerivatives 4.0 International License, which permits any non-commercial use, sharing, distribution and reproduction in any medium or format, as long as you give appropriate credit to the original author(s) and the source, provide a link to the Creative Commons licence, and indicate if you modified the licensed material. You do not have permission under this licence to share adapted material derived from this article or parts of it. The images or other third party material in this article are included in the article's Creative Commons licence, unless indicated otherwise in a credit line to the material. If material is not included in the article's Creative Commons licence and your intended use is not permitted by statutory regulation or exceeds the permitted use, you will need to obtain permission directly from the copyright holder. To view a copy of this licence, visit <http://creativecommons.org/licenses/by-nc-nd/4.0/>.

**Graphical Abstract**



**Introduction**

The skin, the body's largest organ, plays a crucial role in maintaining hemostasis and defending against microorganisms [1, 2]. Skin injuries and wounds can occur due to various factors including lacerations, burns, pressure, diabetes, and infections [3]. While acute wounds typically resolve without complications, chronic wounds, often

resulting from complex diseases or accidents, present a challenge due to delayed healing processes [4, 5]. Diabetic Foot Ulcers (DFU), a form of chronic wound, affect 15%-25% of diabetic patients, with approximately 20% of moderate to severe cases leading to amputation. This significantly impacts both the quality of life and healthcare costs.

The treatment of chronic wounds poses a global challenge due to high costs, increased risk of infection, and elevated inflammation [6–9]. Tissue engineering has emerged as a successful approach for chronic wound healing and skin regeneration. Tissue-engineered grafts, such as biomaterial scaffolds and skin substitutes offer an alternative solution for skin regeneration [10, 11]. Other types of tissue-engineered grafts can include skin substitutes. These skin substitutes are often used in chronic and non-healing wounds and replace the skin function either temporarily or permanently. They can be classified as cellular or acellular. Acellular types, such as dermis tissue without cellular components, include a scaffold or matrix of biopolymers such as collagen or hyaluronic acid. On the other hand, cellular types contain living cells in a matrix, and moreover, these biopolymer components. These cells, like keratinocytes and fibroblasts, can be autologous, allogeneic, and other species. The major categories of skin substitutes include dermal replacement, epidermal replacement, and dermal/epidermal replacement. A variety of skin substitutes are commercially available or in development [12, 13]. Scaffolds play a critical role in enhancing cell retention at the wound site and facilitating cell proliferation, migration, and differentiation within their three-dimensional structures [14, 15]. Effective wound-healing scaffolds must exhibit biocompatibility, biodegradability, and mimicry of the extracellular matrix (ECM). These scaffolds come in various forms such as sponges, nanofibers, and hydrogels [16]. Among these, nanofiber scaffolds have garnered significant attention due to their high surface-to-volume ratio, extensive porosity, ECM-like architecture, and capacity for delivering various agents [17, 18]. The fabrication of nanofiber scaffolds primarily involves methods such as electrospinning, phase separation, freeze-drying, and extrusion [19, 20]. The nano extrusion method, a novel technique, involves the precise extrusion of a polymeric solution under specific pressure and concentration conditions. This method generates nanofibers with controlled diameter sizes, narrow distribution, and accurate thickness. Our prior research has confirmed the suitability of this method for a wide range of water-based polymers without altering their biological properties [21, 22].

While both synthetic and natural polymers can be employed in nanofiber scaffold fabrication, natural polymers stand out due to their exceptional properties, such

as high biocompatibility, biodegradability, and similarity to biological properties. Chitosan, a natural cationic polysaccharide, boasts attributes ideal for wound healing. It stimulates inflammatory cells, macrophages, and fibroblasts, effectively accelerating wound healing by initiating the proliferative phase [23–25]. Hyaluronic acid, a key ECM component, contributes to inflammation control, cellular migration, and angiogenesis [26]. Collagen plays a pivotal role in wound healing by attracting fibroblasts to the wound site, promoting re-epithelialization and cell growth [27]. Hydrolyzed collagen (HC) with low molecular weight offers a cost-effective solution with heightened therapeutic potential for skin and connective tissue regeneration [28, 29]. The efficacy of collagen-based dressings in treating diabetic foot wounds has been corroborated by prior research [30–32].

Today, researchers are enhancing scaffold efficacy by combining them with cell therapy. Regenerative medicine (RM), encompassing cell therapy, holds promise for treating chronic wounds. Stem cell (MSC)-based tissue engineering has demonstrated success in addressing skin disorders, including Epidermolysis Bullosa (EB), Atopic dermatitis, cutaneous burns, and diabetic foot ulcers [33–35]. EB is a genetic disease and the studies investigating the effects of mesenchymal stem cells for treatment of EB are limited [36–38]. But Atopic dermatitis as a chronic inflammatory skin disease is more common and more studies have evaluated MSC therapy [39–41]. Mesenchymal stem cells (MSCs) are used more frequently than other kinds of stem cells in a wide range of diseases including skin disorders [42]. Previous studies have demonstrated that MSCs have therapeutic potential in chronic wound healing by secreting growth factors, cytokines, and chemokines. During the process of wound healing, MSCs can promote angiogenesis, and tissue remodeling and can modulate the immune responses [43–45]. Allogenic sources of MSCs, such as adipose tissue-derived MSCs (ADMSCs) and placenta-derived MSCs (PLMSCs), have emerged as attractive options due to their availability and therapeutic potential. Both cell types can be efficiently derived from waste surgical residues [46, 47]. ADMSCs have immunomodulatory effects and can secrete many growth factors, such as vascular endothelial growth factor (VEGF), fibroblast growth factor (FGF), hepatocyte growth factor (HGF), and transforming growth factor- $\beta$  (TGF $\beta$ ) [48–51]. PLMSCs can be cultured in large quantities and show a more proliferative rate and lower immunogenicity compared with MSCs derived from adult tissue [52–54]. However, traditional methods of stem cell therapy, including systemic and intradermal administration, face challenges related to poor cell localization and

viability [55]. So, scientists use various substrates such as biomaterial scaffolds for stem cell delivery [56–58]. In summary, the mechanism of the next generation of nanofiber composite patches for wound healing can be related to nanofibrous structure and its ability to provide an environment close to the extracellular matrix. Indeed the nanofibrous patch is composed of collagen, chitosan, chondroitin sulfate, and hyaluronic acid to closely mimic the flexibility, stiffness, and adhesiveness of human skin. Biomaterials can act as cell carrier tools that can influence cell behavior. So this patch contains mesenchymal stem cells that can represent paracrine mechanisms of MSC to promote wound healing. The main molecular mechanism in MSC for diabetic wound healing is the ability of MSC to secrete angiogenic growth factors, immunomodulatory factors, and remodeling molecules, that can increase re-epithelialization, granulation tissue formation, and neovascularization in the wound bed [14, 59].

In this study, we have developed a cellular extruded nano-bioscaffold, that represents the next generation of nanofiber composite patches for chronic wounds using a simplified extrusion method. Notably, we focused on the immobilization of MSCs on this novel extruded nano-bioscaffold. Initially, we aimed to create a bioscaffold using entirely natural polymers, including chitosan as the main polymer, hyaluronic acid, hydrolyzed collagen, and chondroitin sulfate, through the nano-extrusion method. Subsequently, we assessed their physical and chemical properties and cell attachment to determine the optimal composition. Then we loaded ADMSCs and PLMSs on the fabricated nano-bioscaffold. Finally, we evaluated the therapeutic effects of the prepared optimized cellular and acellular nano-bioscaffold on diabetic wounds in rat models. This aim was to assess the diabetic wound treatment efficacy of ADMSCs and PLMSCs onto a nanofibrous bioscaffold. Our findings unequivocally demonstrate that our novel cellular nano-bioscaffold outperforms the acellular version. Moreover, PLMSCs/nano-bioscaffold exhibited superior wound healing than ADMSCs/nano-bioscaffold.

## Materials and methods

### Materials

The medium molecular weight (MMW, 190–310 kDa) chitosan (CS) and Hyaluronic acid sodium salt were supplied from Sigma-Aldrich (USA). The hydrolyzed Collagen Type I from bovine Achilles tendon and Chondroitin Sulfate (medical grade) were purchased from Pub Chem (USA). Glacial acetic acid and Ethanol were purchased from Merck (Germany). Fetal bovine serum (FBS), Low glucose Dulbecco's modified eagle medium (DMEM), Phosphate-buffered saline (PBS), Antibiotic–Antimycotic (100X), and Trypsin–EDTA were from Biowest (France). Oil Red O, Alizarin Red S, 1-Ethyl-3-(3-dimethylaminopropyl) carbodiimide (EDC), N-hydroxysuccinimide(NHS), 3-(4,5-dimethylthiazol-2-yl)-2,5-diphenyltetrazolium bromide (MTT), Pico-Sirius red, Rhodamine phalloidin stain, 4',6-diamidino-2-phenylindole (DAPI), streptozotocin (STZ), ketamine, xylazine, and Dimethylsulfoxide (DMSO) were purchased from Sigma-Aldrich (USA). Adipogenesis differentiation kits were supplied from Invitrogen (USA). Lyophilized bovine collagen type I was prepared By the Pasteur Institute of Iran (Iran).

### Ethical considerations

The project was approved by the IRB of the Institute of Pharmaceutical Science, Tehran University of Medical Sciences, Tehran, Iran (Approval ID: IR.TUMS.TIPS.REC.1397.084, Approval Date: 2018–11-06). Placenta and adipose tissue donation were done after obtaining written informed consent from the donors. All Animal experiments were done according to the “Guideline for the Care and Use of Laboratory Animals in Iran” (<https://ethics.research.ac.ir/docs/pages/Guideline-En.pdf>).

### Composite nanofibrous scaffolds preparation

The nanofibrous scaffolds were prepared according to the extrusion process described in our previously published article [22]. Briefly, the chitosan polymeric solution (3% w/v) was prepared by dissolving chitosan in acetic acid 1% (v/v). Other polymeric solutions (collagen, hyaluronic acid, and chondroitin sulfate) were separately prepared by adding the specific amount of each polymer to

**Table 1** The volume ratio of chitosan, collagen, hyaluronic acid, and chondroitin sulfate in nanofiber scaffolds

| Polymer             | Solvent          | Concentration (w/v) % | CS80 portion (%) | CS70 portion (%) | CS60 portion (%) | CS50 portion (%) |
|---------------------|------------------|-----------------------|------------------|------------------|------------------|------------------|
| Chitosan            | Acetic acid (1%) | 3                     | 80               | 70               | 60               | 50               |
| Collagen            | Deionized water  | 1                     | 10               | 10               | 20               | 30               |
| Hyaluronic acid     | Deionized water  | 1                     | 5                | 10               | 10               | 10               |
| Chondroitin sulfate | Deionized water  | 1                     | 5                | 10               | 10               | 10               |

the deionized water (concentration of each one: 1% w/v). Then, the polymeric composite solutions were prepared by mixing these polymer solutions with different volume ratios (Table 1). To obtain our fibrous nano-bioscaffold, the biopolymeric solutions were passed under constant pressure (1–2 bar) through a membrane with 200 nm pore size and time takes less than 3 min. The final nanofibrous composite was dried in an oven (45 °C) for 12 h. The scaffolds were immersed in pure ethanol. Then it was transferred to ethanol 70% / NaOH (1 M) for neutralization and stabilization of the structure of the scaffold. Afterward, the scaffolds were washed with distilled water three times until the pH reached 7. The final product dried at room temperature for 2 days. The processed scaffolds were stored in a refrigerator for further use.

### Physicochemical characterization of scaffolds

#### FTIR spectroscopy

The intramolecular interactions of nanofibrous scaffolds were evaluated by Fourier transforms infrared spectroscopy (670 FTIR, NEXUS Company) in the wavelength range of 400–4000  $\text{cm}^{-1}$  after preparing KBr pellets.

#### Field emission scanning electron microscopy

The morphology of fabricated nanofibrous scaffolds was examined by Field emission scanning electron microscopy (FESEM) (Zeiss Ultra-Plus). For this purpose, some small pieces of prepared scaffolds were put onto the metal stub with proper adhesive. To eliminate the charge conductivity of samples, they were coated with a gold layer under vacuum [60].

#### Atomic force microscopy

The surface topography of the scaffold was investigated by the atomic force microscopy (AFM) method by using an XE-100 instrument (Park Systems, Suwon, Korea) in contact mode. For this purpose 1 cm × 1 cm piece of the fabricated scaffold was attached to the mica surface like other papers [61].

#### Contact angle

The hydrophilicity and hydrophobicity of the scaffold surface were determined by the water contact angle test based on the sessile drop method. The angle formed between the scaffold and the water drop (50  $\mu\text{l}$ ) on the surface was calculated using protractor software [62].

#### Water content

For measuring the water content of the fabricated scaffolds, they were put into the oven at 110 centigrade until constant weight. This procedure was repeated three times. Accordingly, water content (%) was calculated with the formula of ((the initial weight of each sample—the

dried weight of sample)/ initial weight of each sample) [63].

#### Gel fraction

For the measurement of gel fraction, two dried samples (CS80, CS70) were weighed before ( $w_0$ ) and after ( $w_i$ ) immersion in 5 ml deionized water for 8 days. On days 4 and 8 samples were weighed by a digital balance (Kern, Germany, accuracy of 0.0001 g). The gel fraction was calculated with the following Equation:

$$\text{Gel fraction (\%)} = (w_0/w_i) \times 100 \quad (1)$$

#### Swelling study

The swelling behavior of the fabricated scaffolds was investigated at a specific time interval to reach equilibrium. The specified weight of the completely dried scaffolds was immersed in PBS and incubated at 37 °C. At each time point interval, the weighting of the scaffolds was measured by a digital balance. They were taken out of the solution and removed the water from the scaffold surface with a paper towel. The swelling percentage of scaffolds was calculated by the following formula:

$$\text{Swelling (\%)} = [(W_w - W_d)/W_w] \times 100 \quad (2)$$

According to the formula,  $W_w$  and  $W_d$  are the weights of wet and dry scaffolds, respectively.

#### Biodegradation study

In vitro, enzymatic degradation was done by weighing dry scaffolds and immersion and incubation in PBS containing lysozyme solution (0.5 mg/ml) at 37 °C. The weight of samples was evaluated after vacuum drying in 7-day intervals for 28 days [64]. The enzymatic solution was changed every week. The biodegradation percentage was calculated as follows:

$$\text{Biodegradation (\%)} = [(W_0 - W_t)/W_t] \times 100 \quad (3)$$

where  $W_0$ =the initial weight of the scaffold;  $W_t$ =the weight of the scaffold at each time point.

#### Mechanical testing

The mechanical properties (Tensile strength and elongation at break) of scaffolds (10 mm width, 20 mm length) were analyzed by a texture analyzer (Stable Micro Systems Ltd., UK) at the crosshead rate of 1 mm/min according to a standard method for thin films (ASTM D882-12).

#### In vitro study

##### Isolation and expansion of MSC

Adipose and placenta tissues were used as sources of MSCs. In fact, residues of lipoaspiration



surgery (<40 years old) as adipose tissue and full-term (>38 weeks) caesarian section as placenta tissue were harvested from healthy donors. Also before tissue harvesting, laboratory tests were done for screening of blood samples of the donors.

**Isolation and Culture of PLMSCs** PLMSCs were isolated according to the previous protocol [65]. Details of the isolation and culture of PLMSCs from placenta tissue were given in section S1 in Supplementary Data. The PLMSCs at passages 3–5 were used for further in vitro and in vivo studies.

**Isolation and Culture of ADMSCs** ADMSC was manufactured based on the protocol presented previously [66]. Details of isolation and culture of ADMSCs from Adipose tissue were provided in section S2 in Supplementary Data. The ADMSCs at passages 3–5 were used for in vitro and in vivo studies.

#### **MSC characterization Multilineage differentiation of MSCs**

StemPro<sup>®</sup> Osteogenesis and Adipogenesis Differentiation kits were used to induce Osteogenic and adipogenic differentiation, respectively. A detail of the staining process was given in section S3 in Supplementary Data.

#### **CD markers expression of MSCs**

To evaluate the surface markers expansion was used flow cytometry method. Cells were detached from the flask and washed by adding PBS and centrifuged at 1500 RPM for 5 min.  $10^5$ – $10^6$  cells in 100  $\mu$ l PBS were added to each tube. (Unstained Control, CD45/CD34 and CD105/CD73/CD90). An appropriate amount of antibodies were added then mixed gently and incubated at 4 °C for 30 min. Tubes were washed by adding 500  $\mu$ l PBS and centrifuged at 1500 RPM for 5 min. The supernatant was removed and 250  $\mu$ l PBS was added. Samples were run by BD FACS Calibur<sup>™</sup> Flow Cytometer in SABA Biomedicals Co (Tehran, Iran) and FCS files were analyzed by FlowJo software (version 7.6.1). Details of procedure were provided in section S4 in Supplementary Data. The used antibody in the analysis included CD45-FITC/CD34-PE Dual Color Antibody (Cat: 341,071 BD Biosciences), CD73-PECY7 (Cat:344,009 BioLegend Co), CD90-APC (Cat:328,113 BioLegend Co), and CD105-PE (Cat:323,205 BioLegend Co).

#### **Cell Seeding**

The scaffolds were cut into circles with 15 mm diameter, disinfected by 70% ethanol and UV irradiation, and thoroughly washed three times with PBS [67]. Then scaffolds were placed onto a 24-well plate, soaked in 1 ml culture media, and incubated at 37 °C / 5% CO<sub>2</sub> for 2 h. Then,

the medium was removed and the scaffolds were fixed using sterile silicone O-rings. Meanwhile, ADMSCs and PLMSC at passage 3 were trypsinized, centrifuged, and resuspended in culture media at a density of  $5 \times 10^4$  cells. For each well, 200  $\mu$ l of cell suspension was gently added to the scaffold, and the culture plate was incubated at 37 °C / 5% CO<sub>2</sub> for 1 h. Afterward, 300  $\mu$ l culture media was gently added to each well and the plates were incubated for 3 days. Cell attachment on the scaffolds was studied using SEM and PI-DAPI staining.

#### **Collagen Coating and Picrosirius red staining**

The sterilized round-shaped scaffolds were immersed in PBS for 30 min, after removing PBS, 1 mg/ml collagen type I was coated on the surface of the scaffolds for 2 h at 4 °C. The EDC/ NHS solution was prepared in 95% ethanol to immobilize collagen on the surface, and the EDC/ NHS solution (at a ratio of 2:1) was added to scaffolds (4 h at room temperature). After the completion of the immobilization process, the scaffolds were washed with PBS three times [68]. To examine the collagen immobilization Picro-Sirius Red (PSR) staining was used. The PSR staining solution (1 mg/ml) was prepared by dissolving Sirius Red F3B in saturated aqueous picric acid. Samples were immersed in PSR staining solution for 1 h, were intensively washed with distilled water several times, and dried. The stained collagen was observed under an inverted light microscope and photos were taken using a digital camera (Nikon, Japan). For staining quantification, samples were immersed in 0.5 M NaOH for 2 h and the absorbance of the extracted solution was assessed at 540 nm by UV–VIS spectrophotometer [69, 70].

#### **Cell attachment assay**

The scanning electron microscope (TESCAN model MIRA3, Czech Republic) was used for assessing MSCs' attachment after 3 days and the stability of cell attachment onto the scaffolds after 5 days. To evaluate the morphology of attached cells, an inverted microscope was used. For fluorescence imaging, the cells-seeded scaffolds were fixed in 4% paraformaldehyde for 20 min (at room temperature), then washed three times with PBS, and permeabilized with 0.1% Triton X-100 for 10 to 20 min. To stain actin filaments, Phalloidin solution was added and the samples were incubated at room temperature for 2 h. Nuclei were counterstained with DAPI (20 min at room temperature). The samples were examined by an inverted fluorescence microscope (Olympus IX-81). Cell attachments were quantified with Image J software. MSC nuclei onto the CS80 and CS70 scaffolds were counted in 4 different fields of 0.25 mm [71].

### **Cytotoxicity assay**

MTT assay was done to assess the cytotoxicity of the scaffolds [72]. Briefly, scaffolds were placed in 96 well plates and 20  $\mu$ l MSCs suspension containing cells were seeded into each well. After 1 h incubation, 100  $\mu$ l culture media was gently added per well and the culture plates were incubated at 37 °C/5% CO<sub>2</sub> for 1, 3, and 5 days. The MTT solution was prepared by dissolving MTT powder in PBS at 5 mg/ml concentration. After the incubation period, the media was removed, a mixture of 20  $\mu$ l MTT solution / 80  $\mu$ l culture media was added per well, and the plates were incubated at 37 °C with 5% CO<sub>2</sub> for 4 h. Then the supernatant was replaced with 100  $\mu$ l DMSO and the plates were shaken slowly for 5 min to dissolve the formazan crystals. The supernatant was transferred to an empty plate and optical absorbance was read at 570 nm by a microplate reader. The control group was the well without scaffolds.

Endotoxin levels of fabricated scaffolds were assayed using the Limulus Amebocyte Lysate (LAL) test with the Gel-clot method (ISO 10993–11:2017: Tests for material-mediated pyrogens in medical devices). The LAL test method (sensitivity of 0.01 EU/mL) was done by the KiaNanoBioVista laboratory (Tehran, Iran).

### **In vivo study**

#### **Experimental diabetic rat model**

In this study, all animal experiments were carried out following the guidelines and regulations related to the care and use of laboratory animals presented by the animal ethics committee of Tehran University of Medical Sciences (Code No. IR.TUMS.TIPS.REC.1397.084). Also, the animal study was reported in line with the ARRIVE guidelines 2.0. Forty male Wister rats (weighing 200–250 gr, 8–10 weeks old) were purchased from the Pasteur Institute (Tehran, Iran). All rats were placed in a room under a 12-h light–dark cycle and controlled temperature and humidity. The health status of rats was monitored daily by the relevant expert. Diabetes was induced in rats with a single dose injection of 60 mg/Kg STZ in sodium citrate buffer (pH4.5) intraperitoneally [73]. Before STZ injection, the animals fasted for 12 h and according to the standard chow ad libitum diet and water, they were fed. The blood sugar levels of the rats were monitored for 30 days daily by a glucometer device (BEURER GL42, Germany). The blood sugar higher than 160 mg/dL was considered as diabetes.

#### **Surgical procedures**

For anesthetizing of all diabetic rats, intraperitoneally used ketamine (100 mg/kg) and xylazine (10 mg/ kg). The excisional wound model was created according to

a previously described method [74]. Briefly, the dorsal skin hair was shaved and using 70% ethanol and povidone-iodine disinfected. A punch biopsy instrument was used to create a 2 cm round-shaped wound on the dorsum of each rat. After surgery, the animals were randomly placed in four groups including the PLMSC/Scaffold group (CS70-P), ADMSC/Scaffold group (CS70-A), scaffold group (CS70), and the control group (without any treatment) using the RAND() function in Microsoft Excel. Single blinding was implemented for researchers responsible for conducting animal experiments and analyzing histopathology.

#### **Wound closure rate**

To assess the wound healing rate, the photographs were taken by a digital camera at a certain time interval: 0, 7, 14, and 21 days post-treatment. To measure the wound area, pictures were analyzed with Image J software (NIH, USA). The wound closure rate was calculated according to the following formula:

$$\text{Rate of Wound Closure} = ((A_0 - A_t) / A_0) \times 100 \quad (4)$$

$A_0$  = area of the original wound at day 0,  $A_t$  = area of the wound at day t.

#### **Histopathology analysis**

The biopsy of the wound site from each group was collected at days 7 (n=3), 14 (n=3), and 21 (n=3) post-treatment. For this purpose, animals were euthanized. For animal euthanasia were used ketamine (500 mg/kg) and xylazine (50 mg/ kg). After that, the wound site was cut by a scalpel, and the harvested tissues were immediately fixed in the 10% neutral buffered formalin (pH=7.26) for 48 h. The fixed tissue samples were embedded in paraffin. To prepare the paraffin blocks, the tissue was transferred to the tissue preparation device where the steps of dehydration and clarification were done. After 24 h, the tissue was removed from the device and molded in paraffin blocks. After cooling the molds, slices with 5  $\mu$ m thickness were prepared using a microtome machine (Leica RM2135 Rotary Microtome). The slices were covered on a glass slide. Tissue sections were stained with hematoxylin & eosin (H&E) and Masson's trichrome (MT) according to the manufacturer's instructions. The histological samples were evaluated by an independent reviewer by light microscopy (Olympus BX51, Japan). Angiogenesis, inflammatory cell infiltration, and collagen content were assessed and compared in different groups. The different cells were counted in 400X magnification within five field repetitions and the average was calculated. Epithelialization was assessed on 7, 14, and 21 days post-treatment semiquantitatively on 3 microscopic slides: 0 (without

new epithelialization), 1 (25%), 2 (50%), 3 (75%), and 4 (100%) epithelialization.

**Statistical analysis**

All experiments were done in triplicates. The results were expressed as mean ± standard deviation. The results were analyzed statically by Graph Pad Prism software (version 9.4.1). The statistical comparisons were applied using a t-test, one- or two-way analysis of variance (ANOVA), and Tukey’s multiple tests. Significance was indicated

at  $p < 0.05$  for all statistical tests. ( $*p < 0.05$ ,  $**p < 0.01$ ,  $***p < 0.001$ ,  $****p < 0.0001$ ).

**Results**

**Morphological properties**

The morphology of different extruded scaffolds (CS80, CS70, CS60, and CS50) was studied by FESEM and AFM. The SEM images of CS80, CS70, CS60, and CS50 scaffolds are displayed in Fig. 1. As shown the nanofiber diameters for CS80, CS70, CS60, and CS50

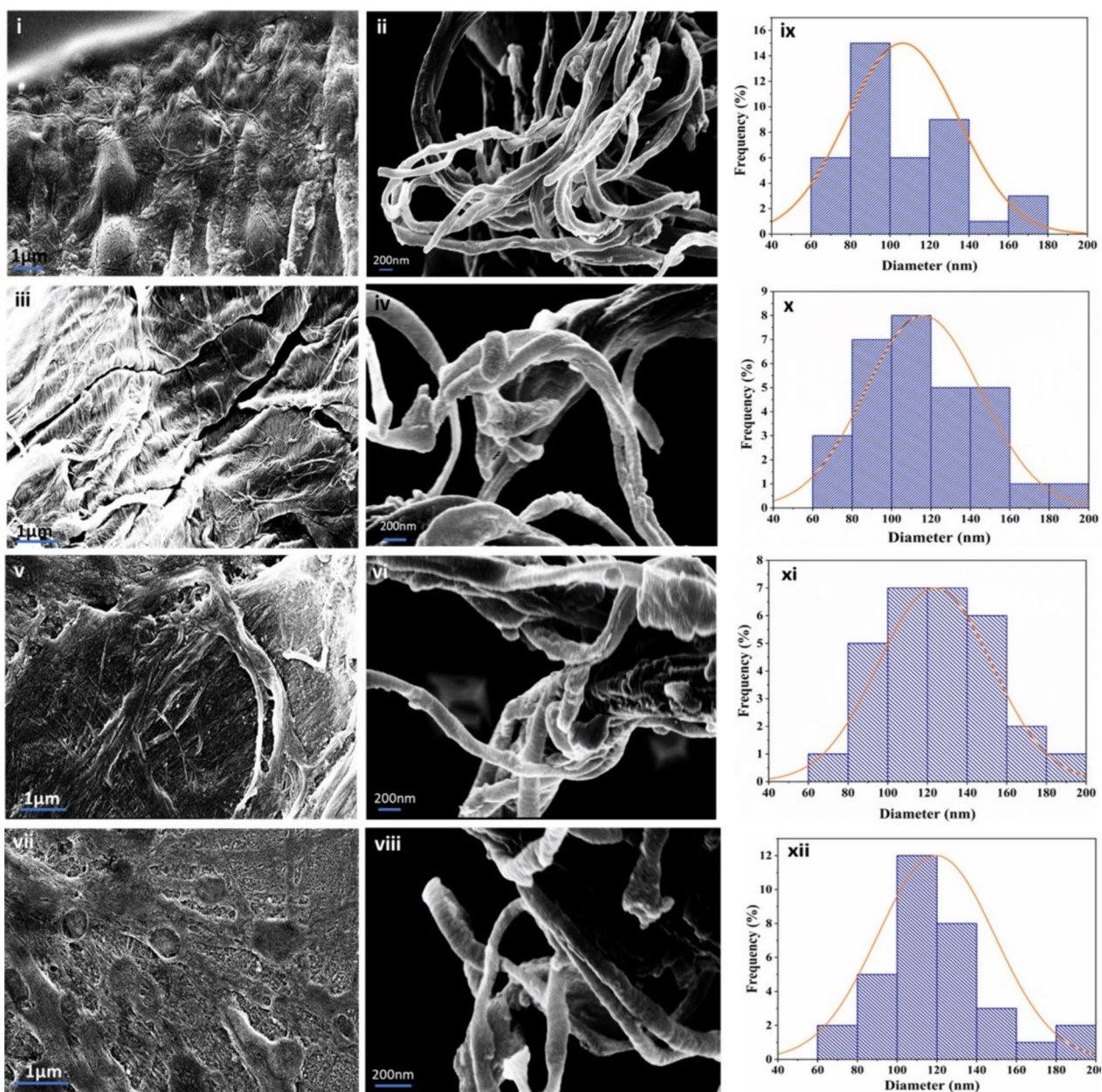


**Fig. 1** Morphology analysis- SEM imaging of extruded nanofibers composite scaffolds, (i, ii) CS70, (iii, iv) CS80, (v, vi) CS60, (vii, viii) CS50, scale bars 200 nm, 1 μm. (ix,x, xi,xii) Nanofibers diameter distributions for CS70, CS80, CS60, and CS50, respectively



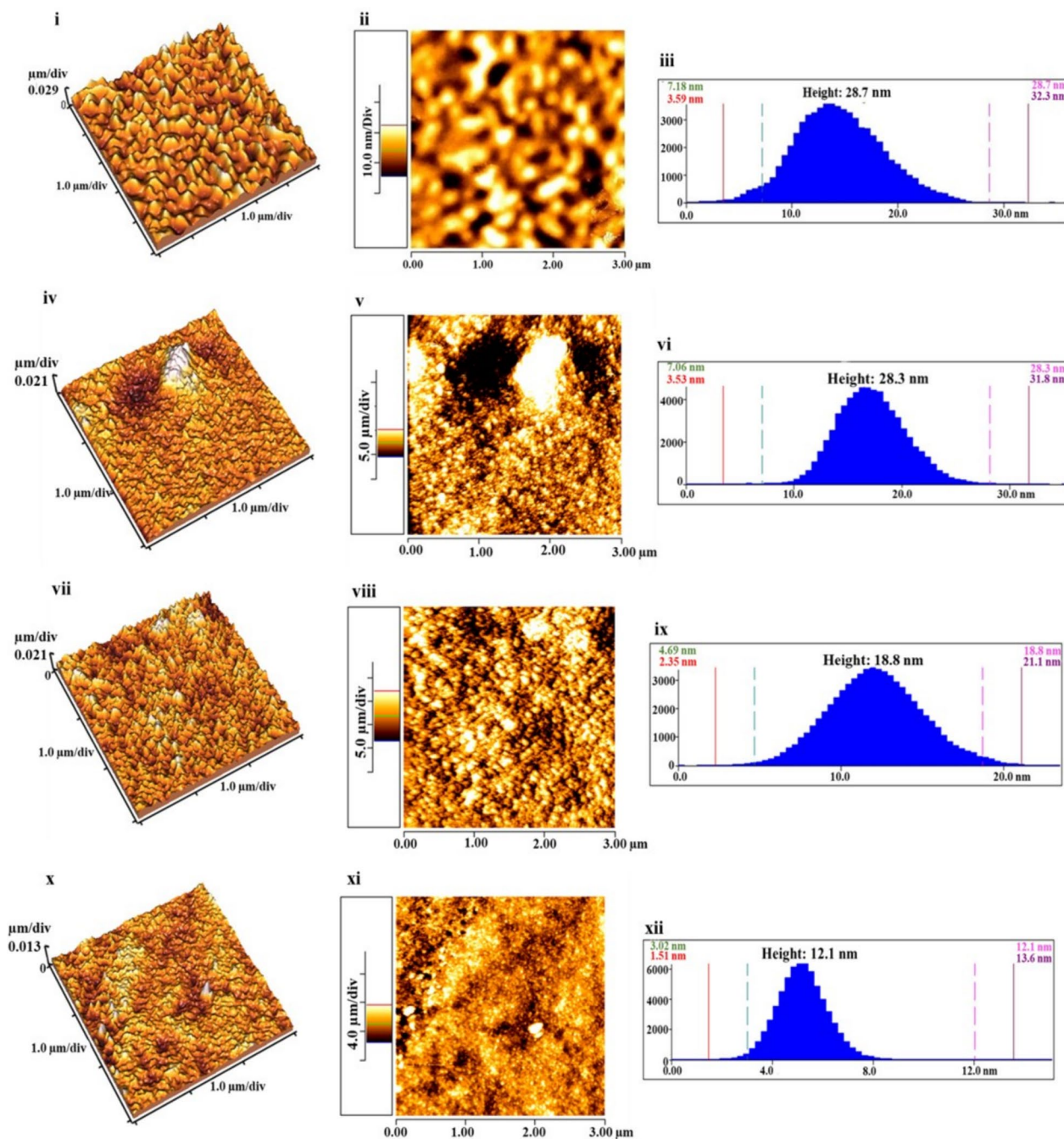


**Fig. 2** Morphology analysis: (i, ii, iii) 2D and 3D AFM imaging of CS70, (iv, v, vi) 2D and 3D AFM imaging of CS80, (vii, viii, ix) 2D and 3D AFM imaging of CS60, (x, xi, xii) 2D and 3D AFM imaging of CS50. (scan size  $1 \times 1 \mu\text{m}$ )

were measured  $116 \pm 29$  nm,  $106 \pm 28$  nm,  $128 \pm 27$  and  $119 \pm 30$ , respectively. The analysis of the fiber dimension was measured by Image J software (v1.018). At least 40 diameters were measured by image J, for evaluating the error in nanofiber diameter. The AFM pictures of CS80, CS70, CS60, and CS50 scaffolds are presented in Fig. 2. The results indicated that the nanofibers had a surface

roughness of less than 5 nm and therefore confirmed the surface uniformity and the elimination of drying effects.

#### Physicochemical properties

At first the CS80 and the CS70 as the main scaffolds were fabricated and assessed their physico-chemical characterization. FTIR spectrometer was employed

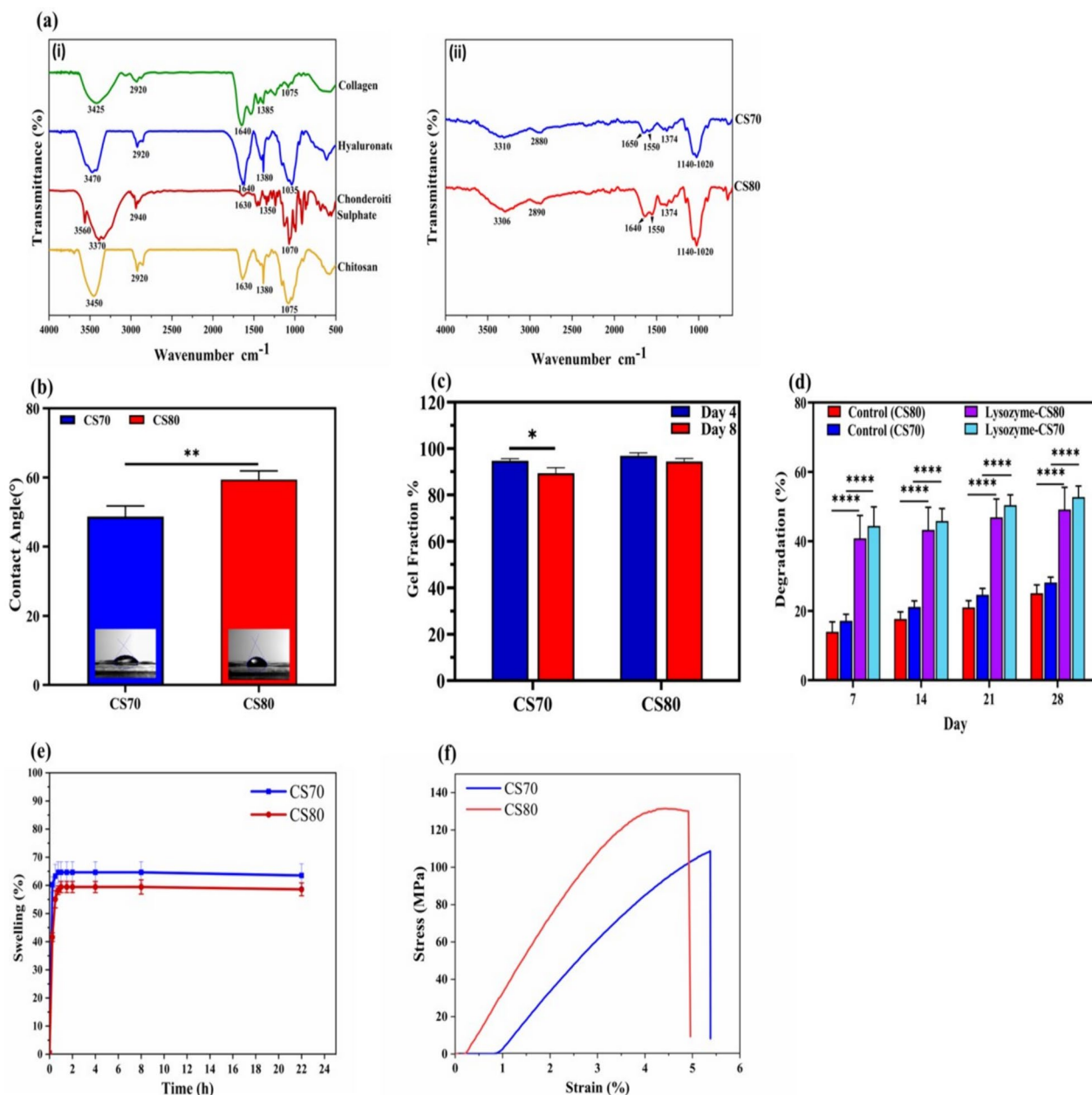


**Fig. 3** Physicochemical characterization of CS80 and CS70. **a** FT-IR spectra for (i) Chitosan, collagen, chondroitin sulfate, and hyaluronic acid, (ii) CS80 and CS70 scaffolds. **b** Water contact angle test, (\*\* $p < 0.01$ ), **c** gel fraction. (\* $p < 0.05$ ), **d** Biodegradation rate. (\*\*\*\* $p < 0.0001$ ), **e** swelling percentage in PBS, **f** stress–strain curve of nanofibrous scaffolds CS80 and CS70

for chemical characterization. The results for scaffolds (CS80, CS70) and different polymers (chitosan, collagen, hyaluronic acid, and chondroitin sulfate) have been illustrated in Fig. 3a. The FTIR patterns of scaffolds (Fig. 3a) are similar to the chitosan one, due to chitosan having the highest portion in the scaffold composition. In the composite scaffolds, the carbonyl band has overlapped with the amide I band, Due to the presence of higher

chitosan than others. The stretching vibrations of the O–H ( $3310 \text{ cm}^{-1}$ ) and N–H ( $3306 \text{ cm}^{-1}$ ) bonds' position and their relative intensities were decreased, due to the interactions between polymers. The observation of frequency shifts towards lower positions and changes in the shape of –OH and –NH bands can indicate the formation of hydrogen bonds in the structure of scaffolds. The surface hydrophobicity and hydrophilicity of nanofibrous

scaffolds are represented in Fig. 3b. The water contact angle of CS70 and CS80 obtained  $48.7^\circ$  and  $59.3^\circ$ , respectively. Water content of the scaffold was measured around 5% which was close to the previous reports [22]. The water contact angle data showed acceptable hydrophilicity of scaffolds which is in accordance with the results of the swelling test. The gel fraction results of scaffolds in aqueous media at day 4 and day 8 are demonstrated in Fig. 3c. The gel fraction of  $94.25 \pm 1.35$  and  $89.55 \pm 204$  on day 8 was measured for CS80 and CS70, respectively. The swelling behavior of scaffolds can influence better oxidation, efficient nutrient transfer, and reduced infection at the wound site. It also affects cell attachment, migration, and proliferation [75, 76]. Figure 3e shows the water adsorption rate of fabricated scaffolds. In the first swelling rapidly increased up to reach near-equilibrium values. After 45 min incubation time, the highest swelling ratio of CS70, and CS80 nanofiber scaffold were obtained which were  $64.63 \pm 3.80\%$  and  $58.28 \pm 1.52\%$ , respectively. The swelling behavior of both scaffolds is almost the same and shows a suitable water adsorption rate. It was shown that high concentrations of enzymes such as lysozyme were present at chronic wound sites. So it is necessary to evaluate enzymatic degradation of scaffolds [77, 78]. Lysozyme, a non-specific mammalian enzyme, can degrade chitosan-based biomaterials through a hydrolysis reaction. Non-toxic products such as oligosaccharides are obtained from the degradation process which can be interacted with and combined with glycosaminoglycan and glycoproteins [79]. Figure 3d illustrates the in vitro degradation of CS70 and CS80 in the presence and absence of lysozyme solution for 28 days. The result showed that in the absence of enzyme, the rate of weight loss for control groups (CS70, CS80) after 28 days is about 28.2% and 25.4%, respectively. In the presence of the lysozyme, the degradation rate was increased ( $p$ -value  $< 0.0001$ ) and the mass loss rate for Ch-80 was 49.17% and for CS70 was 52.76%, after 28 days. Based on statistical evaluation, in all degradation days, the degradation rate of the lysozyme-CS80 and the lysozyme-CS70 were significantly increased compared to CS80 and CS70, respectively. The control group indicated constant degradation via erosion and hydrolysis that did not show remarkable mass loss during 28 days. The increased biodegradation rate can be due to the erosion via hydrolysis of glycoside and amide bonds by lysozyme. Evaluation of mechanical property as a significant parameter for a bio-engineered graft is important to consider the biomechanical principles for cells to bio-mimicking tissue-like graft. The density and distribution of intermolecular and intermolecular interactions in the polymeric network of film scaffolds can be affected by their mechanical properties [60, 80]. The stress-strain curve is represented in Fig. 3f.

Maximum stress at the breaking point and the elongation at the breakpoint (Eb %) were 125.34 MPa and 5.55% for CS80, and 108.7 MPa and 5.35% for CS70.

#### MSCs characterization

To confirm the isolated cells possess phenotype characteristics for MSCs, their morphology, surface markers expression, and Osteogenic and adipogenic differentiation were evaluated. (Figure S1 and sections S5, S6, and S7).

#### Cell behavior on the surface

It considered cell adhesion is the first step of communication between cells and substrate in the field of RM and tissue engineering. Attachment of cells on the surface can affect cell activities such as cell proliferation, migration, and differentiation [81–83]. Cell adhesion was investigated by culturing the PLMSC and the ADMSCs on the surface of our fabricated scaffolds. For this purpose, various techniques such as using a cell strainer, silicone O-Ring for fixing scaffolds and preventing cell escape, and surface modification with  $O_2$  and air plasma were applied. Cell attachment was assessed by observing under an optical microscope and DAPI staining after 1 day. As shown in Figure S2 (section S8), no cells were attached to the surface of the prepared scaffolds after DAPI staining. The CS60 and CS50 scaffolds were prepared to evaluate the MSCs' attachment to the surface by changing the chitosan and collagen portion in the composition of the scaffolds (Table 1). It is known that increasing the amount of collagen type I in the structure improves the attachment of cells to the material's surface [84, 85]. Also Figure S2 confirmed no cell attached to all scaffolds (CS80, CS70, CS60, and CS50). In this study, it can be concluded that reducing the amount of chitosan and increasing the amount of hydrolyzed collagen in the scaffold composition cannot improve cell attachment. So for the achievement of the cellular scaffold, another technique, the coating of the surface with collagen type I (triplex structure) was chosen. Figure 4a, b shows the DAPI staining and optical microscope images taken of the cultured cells onto the collagen-coated samples (CS80 and CS70) after 1 day of cultivation. According to these images, cells were attached to the scaffolds successfully. The quantification of cell attachment is shown in Fig. 4c. Also, the attachment of PLMSC onto the CS70 was evaluated on days 1, 3, and 5 after cell seeding with an optical microscope (Figure S4). The attachment of the MSCs onto the CS80 and CS70 was also assessed by SEM technique (Fig. 5). Following the results, collagen-coated scaffolds are well able to load cells onto themselves. Also, the stability of cell attachment on the collagen-coated CS70 as a desirable scaffold was assessed by SEM after 5 days



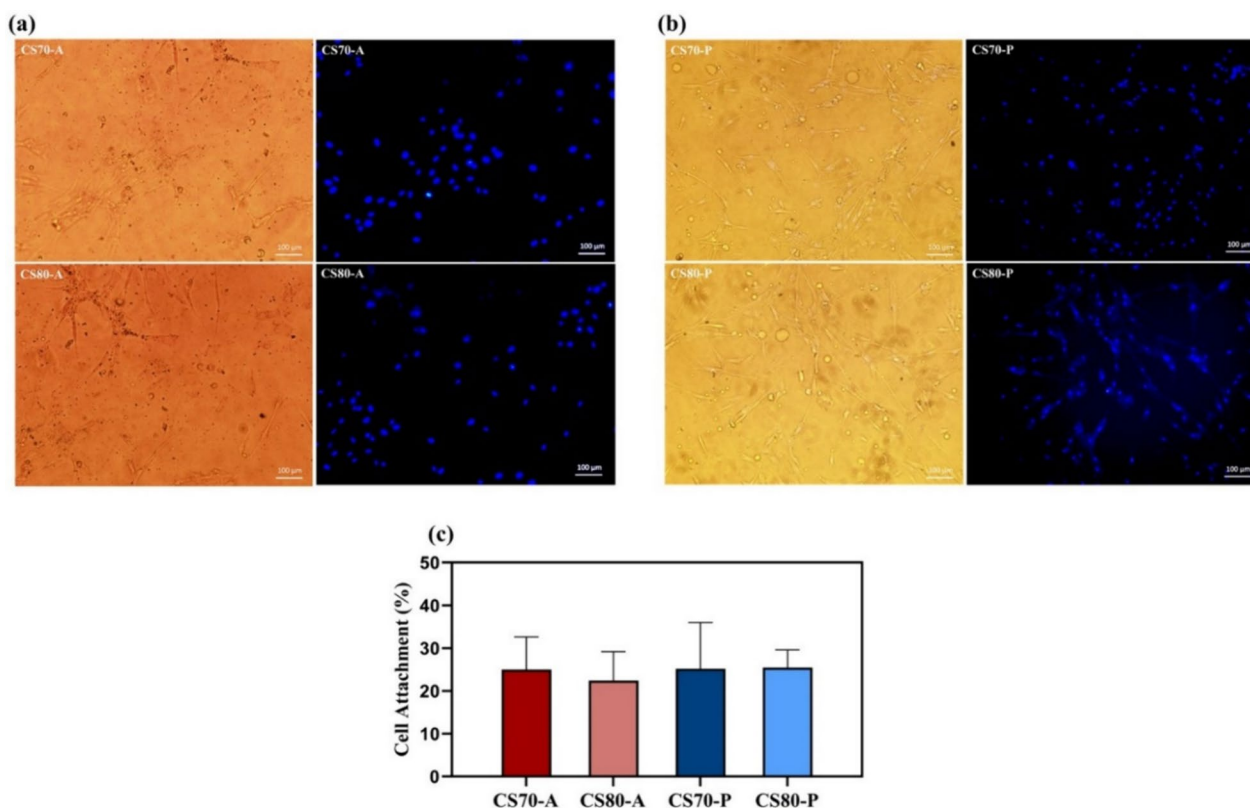


**Fig. 4** MSCs attachment on the collagen-coated scaffolds. **a** DAPI staining and optical microscope images of collagen-coated CS80 and CS70 scaffolds after 1 day of ADMSCs seeding - (CS80-A and CS70-A), **b** DAPI staining and optical microscope images of collagen-coated CS80 and CS70 scaffolds after 1 day of PLMSCs seeding - (CS80-P and CS70-P), (Magnification: 10x). **c** The percentage of MSCs attachment to the CS70 and CS80 scaffolds on day 1

of seeding (Figure S3). Figure 6 represents Rhodamine-phalloidin and DAPI staining of cellular CS70. Because the CS70 scaffold had a better property for our purpose it was chosen for in vivo study. Rhodamine-phalloidin and DAPI staining of PLMSC/CS70 and ADMSC/CS70 shows a uniform shape with little spreading and adhesion phenotype. This result confirmed cell adhesion on the fabricated scaffold. Biochemical staining based on chemical reactions is a simple and inexpensive method. It can be used selectively for staining the substrate's components. Routine staining protocols such as van Giesons, PSR, and a variety of trichrome dyes (Masson, Mallory, and Heidenhain) are used to determine collagen fibrils. However, among these methods, PSR might be a better choice. Because it is a more sensible and selective dye [86, 87]. PSR could bind specifically to collagen fibrils. Figure 7 shows the presence of the collagen fibrils on the scaffold surface by PSR staining. The amount of collagen on the surface was evaluated by SR relative absorbance [70, 88]. The Sirius red OD for scaffolds is shown in Fig. 7a. Observation of collagen fibrils on the surface by optical microscope was exhibited in Fig. 7b. the results

confirmed the presence of collagen fibrils on the surface of the scaffolds. Also, the result indicated no significant difference and the relative OD did not differ notably.

#### Cytotoxicity assay

The biocompatibility of fabricated scaffold supports cell attachment, migration, and proliferation [89]. To assess the cytotoxicity and biocompatibility, an MTT assay was used for different prepared scaffolds. Figure 8 illustrates the results of the MTT assay for coated scaffolds (CS80, CS70, CS60, and CS50) in three time intervals of 1, 3, and 5 days. Based on the results, the prepared scaffolds not only show no cytotoxicity but also they can promote cell proliferation. It can be concluded that the MSCs on our fabricated scaffolds have more viability and have proliferated well in comparison with control groups. LAL test confirmed there was no intact gel formation in sample solutions. Based on the results, the fabricated patch is considered non-pyrogenic (1:100) and satisfies the requirements of the test.



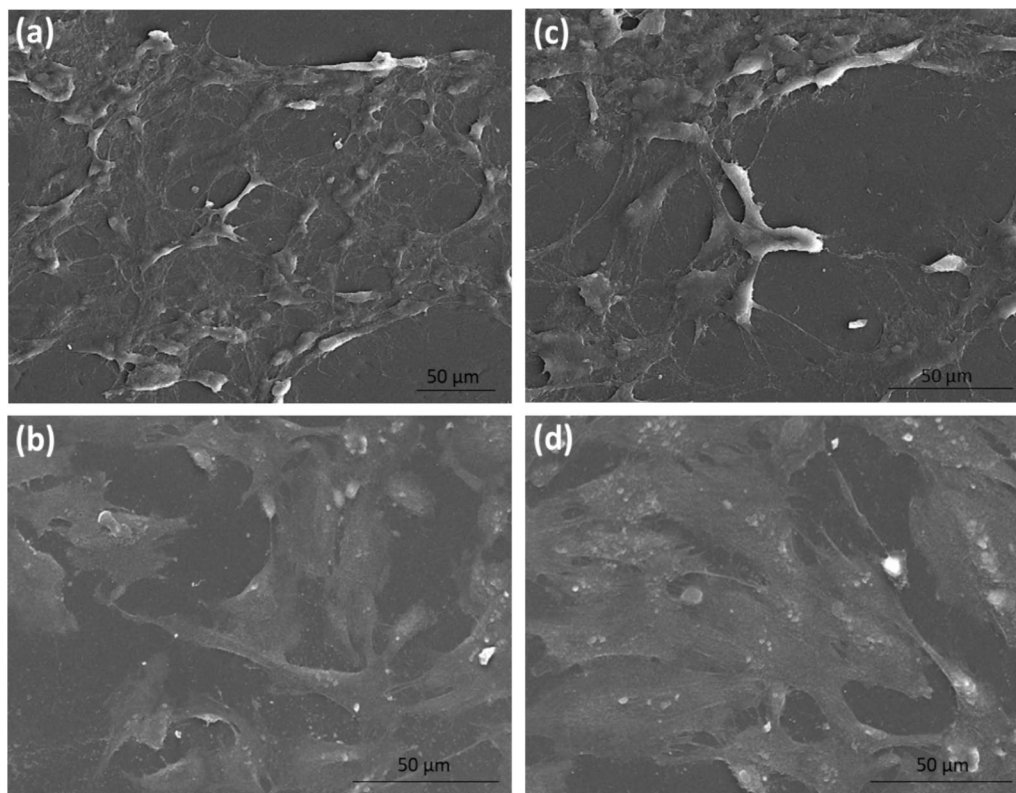


**Fig. 5** SEM images of the collagen coated scaffolds (CS70 and CS80) seeded with mesenchymal stem cells. **a** CS70 seeded with ADMSC (CS70-A), **b** CS70 seeded with PLMSC (CS70-P), **c** CS80 seeded with ADMSC (CS80-A), **d** CS80 seeded with PLMSC (CS80-P) at day 3

## In vivo wound healing

### Rate of wound closure

The effectiveness of cellular and acellular nanofiber scaffolds was evaluated in the diabetic animal model with the excisional wound on the dorsal of each rat. For this purpose, the wound healing process was monitored at 7, 14, and 21 days post-treatment with different cellular and acellular nanofiber scaffolds. Figure 9a displays the photographic images that were taken at mentioned intervals. As seen, the wound size of all groups decreased with increasing treatment time but the groups seeded with cells indicated the highest wound closure rate compared to other groups. Figure 9b shows quantitatively the wound closure rate at the mentioned time intervals. On day 7, the healing rate of placenta/CS70 ( $p < 0.001$ ) and adipose/CS70 ( $p < 0.001$ ) were significantly higher compared with CS70 and the control group. In addition, the wound size of cellular groups (CS70-P and CS70-A) was significantly reduced compared to the control group ( $p < 0.05$ ) after 14 days post-treatment. On day 21, the wound healing rate of CS70-P and CS70-A compared to the control group ( $p < 0.01$  and  $p < 0.05$ , respectively, and CS70-P compared with CS70 ( $p < 0.05$ ) were significantly promoted. So, macroscopic images of wound closure

and the quantitative measurement of wound closure rate indicated the sensible wound healing effect of cellular treatment groups compared to control groups after 14 days (Fig. 9).

### Histopathological analysis

The results of histopathologic studies performed by H&E and MT staining on days 7, 14, and 21 post-treatment are represented in Fig. 10. The control group showed the formation of granulation tissue and a lot of inflammatory cells on days 7 and 14 and the CS70 group was similar to the control group. Moreover, the control group did not show re-epithelialization until 21 days post-treatment. Histopathological studies (Fig. 10) revealed the re-epithelialization process was initiated on day 14. One of the effective parameters that improve the efficiency of wound healing is the number of collagen fibers deposited in the subcutaneous tissue of the wound site. The healing process and granulation formation accelerate with increasing synthesis and deposition of collagen [90, 91]. MT staining exhibited an increase in the collagen fiber deposition on days 14th, and 21th in all the groups (Fig. 10). As seen, the blue color in the CS70-P and

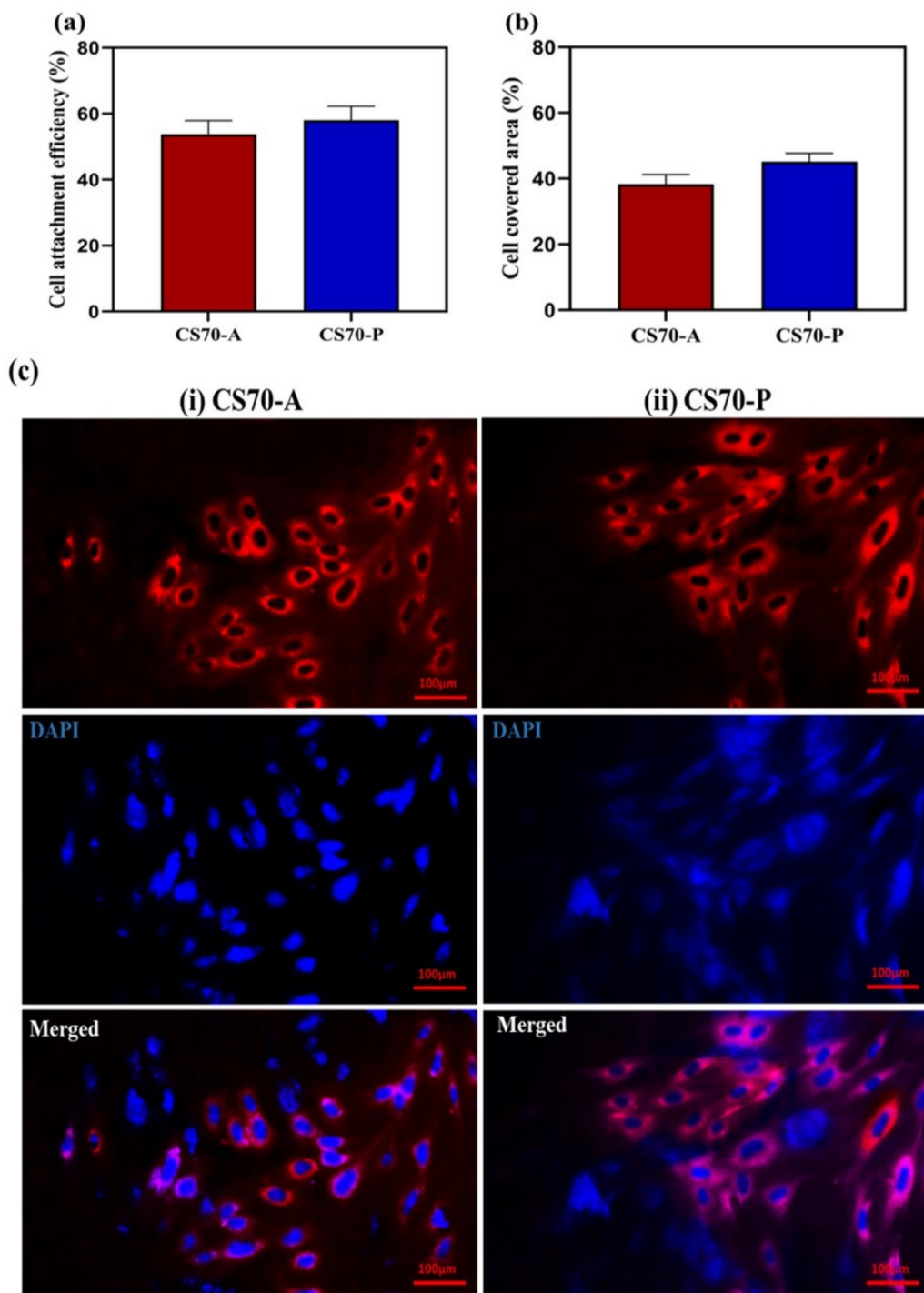


**Fig. 6** Adhesion of ADMSCs and PLMSCs on the collagen coated CS70 scaffold **(a)** number of cells attached to scaffold, **b** MSCs covered area on the CS70 scaffold, The data are presented as the mean  $\pm$  standard deviation, **c** Rhodamine phalloidin-DAPI images of ADMSCs and PLMSCs onto collagen coated CS70 scaffold (i) CS70-A, (i) CS70-P, respectively (at day 3 after cell seeding, scale bar: 100  $\mu$ m, blue and red represents nucleus and Cytoskeleton, respectively)

CS70-A treatment groups was more intense which indicated the collagen deposition in these groups was more compared to other groups, and the same

results were seen in Fig. 11a. Neovascularization and angiogenesis are very important parameters in the tissue remodeling process as ending phases of wound

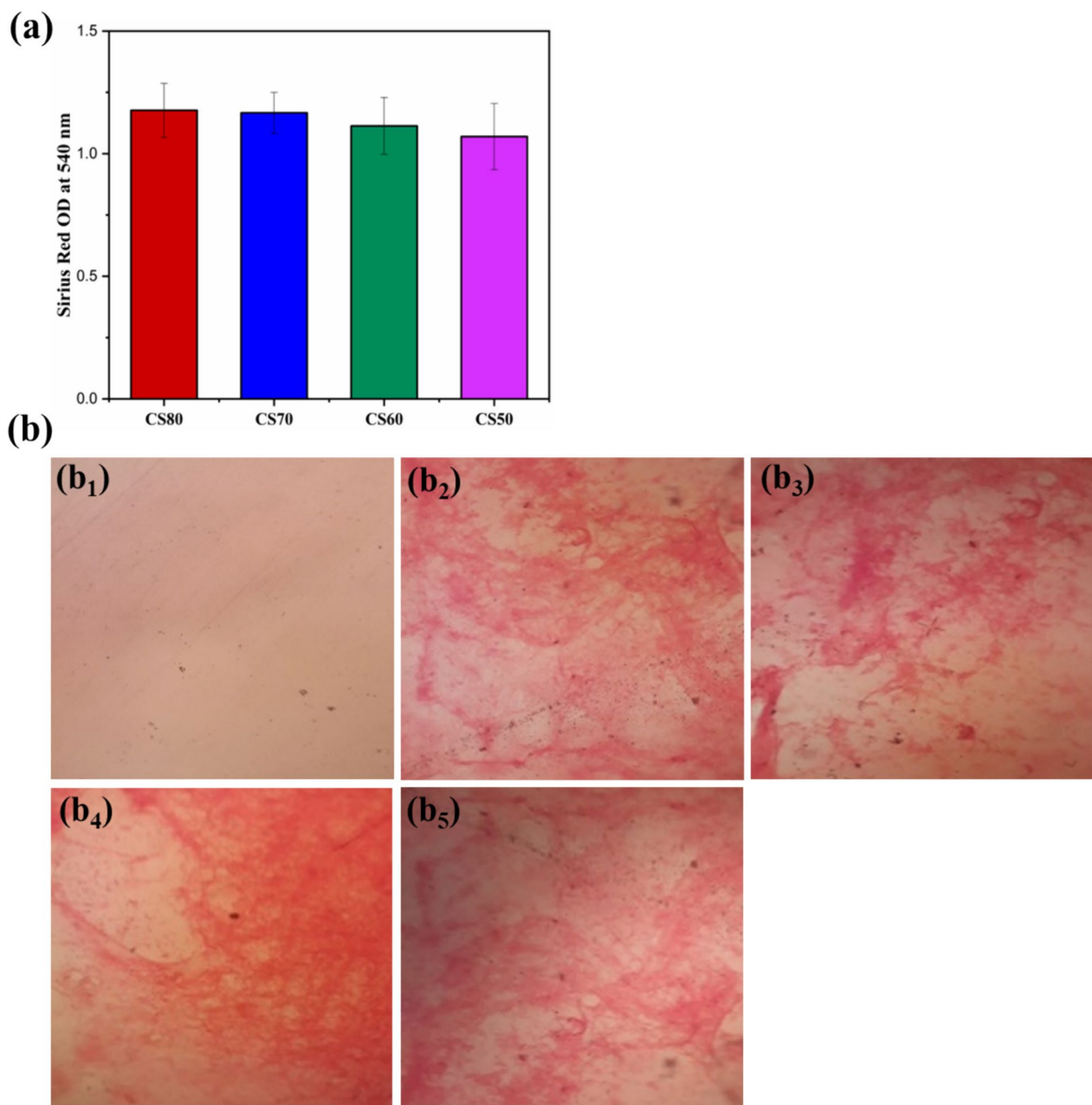


**Fig. 7** Sirius Red staining of collagen-coated scaffolds. **a** Sirius Red OD absorbance of prepared collagen coated scaffolds. **b** Picosirius red staining of collagen-coated onto the CS80 (**b<sub>2</sub>**), CS70 (**b<sub>3</sub>**), CS60 (**b<sub>4</sub>**), CS50 (**b<sub>5</sub>**), and uncoated scaffolds as a control group (**b<sub>1</sub>**). (Magnification: 20×)

healing, Because of the role of the blood vessel in the delivery and infiltration of oxygen, and nutrients to the wound bed [92, 93]. The quantity of collagen density, blood vessels, and the infiltrations of the inflammatory cells in the wound site of different groups at days 7, 14, and 21 post-treatment are exhibited in Fig. 11. As shown in Fig. 11a, the content of collagen deposition increased during the treatment period until day 21 in all groups. Furthermore, the collagen synthesis

did not change significantly in any groups on days 7 and 14. However, the collagen deposition of CS70-P ( $p < 0.01$  and  $p < 0.001$ , respectively) and CS70-A ( $p < 0.05$  and  $p < 0.01$ , respectively) were significantly increased compared with CS70 and the control group after 21 days post-treatment As seen in Fig. 11c, for all groups an extensive infiltration of inflammatory cells was shown until day-7. Then, a decrease in inflammatory cell infiltration for all groups was illustrated after

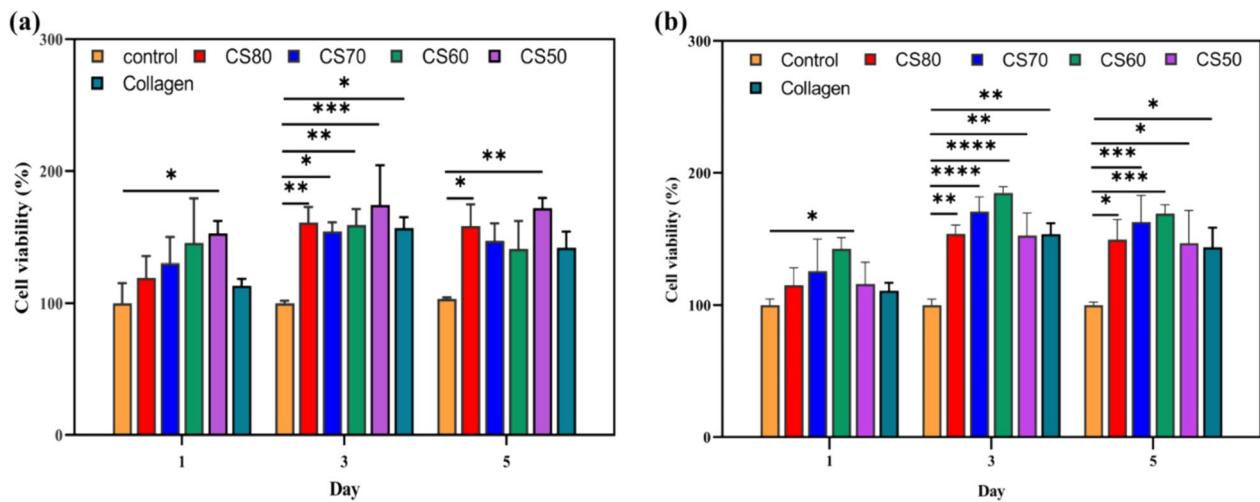


**Fig. 8** The proliferation of MSCs on CS80, CS70, CS60, and CS50 nanofiber scaffolds for days 1, 3, and 5, as determined by MTT assay. **a** PLMSC viability on the coated scaffolds, **b** ADMSC viability on the coated scaffolds, Statistical analysis was done by one-way ANOVA (\* $p < 0.05$ , \*\* $p < 0.01$ , \*\*\* $p < 0.001$ , \*\*\*\* $p < 0.0001$ )

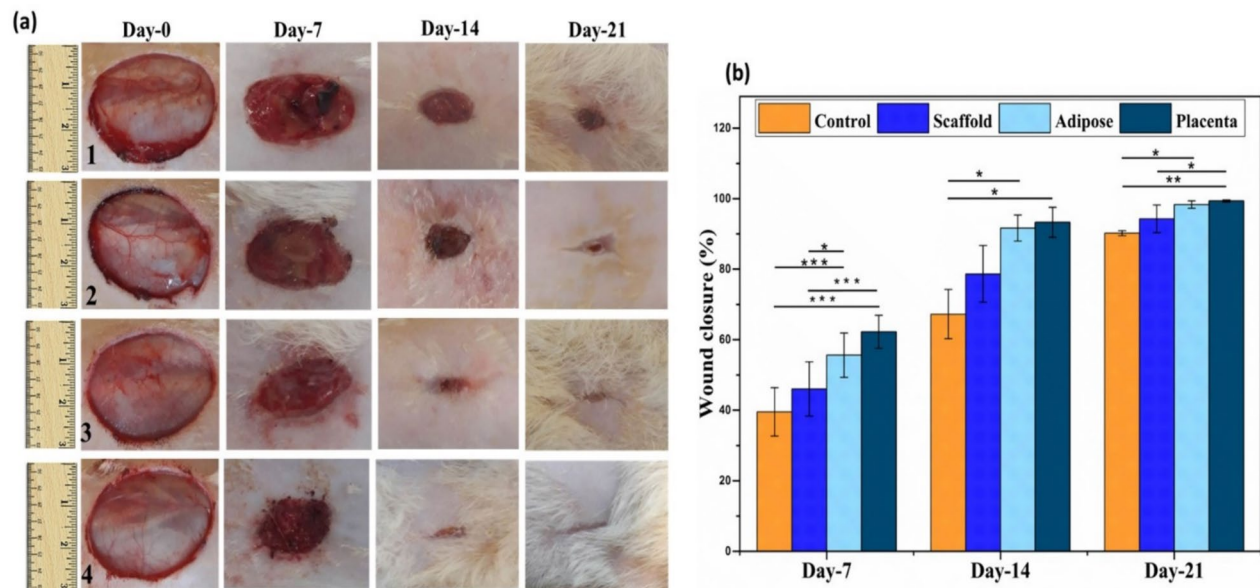


**Fig. 9** In vivo wound healing process. **a** Macroscopic images of the wound on days 7, 14, and 21 post-treatment, (1) Untreated (control), (2) Scaffold (CS70), (3) ADMSC + scaffold (CS70-A), (4) PLMSC + scaffold (CS70-P). **b** Percentages of wound closure at the different time points (7, 14, 21) (\* $p < 0.05$ , \*\* $p < 0.01$  and \*\*\* $p < 0.001$ )

7 days till day 21. Figure 11b represents the quantitative analysis of angiogenesis for all groups at different time intervals (7, 14, and 21 days). On day 7, the highest new blood vessels were formed in the CS70-P group compared to other groups. Figure 11d summarizes the semi-quantitative results of the histomorphometric analysis for all groups on 7, 14, and 21 days post-treatment.

**Discussion**

In general chronic non-healing wounds do not follow the normal wound-healing process and are stuck in different phases of the healing process. Impairment in the healing phases can be related to infection, unresolved inflammation, and failure in the healing process such as angiogenesis, epithelial migration, and cell proliferation [94, 95]. There are many wound dressers for the



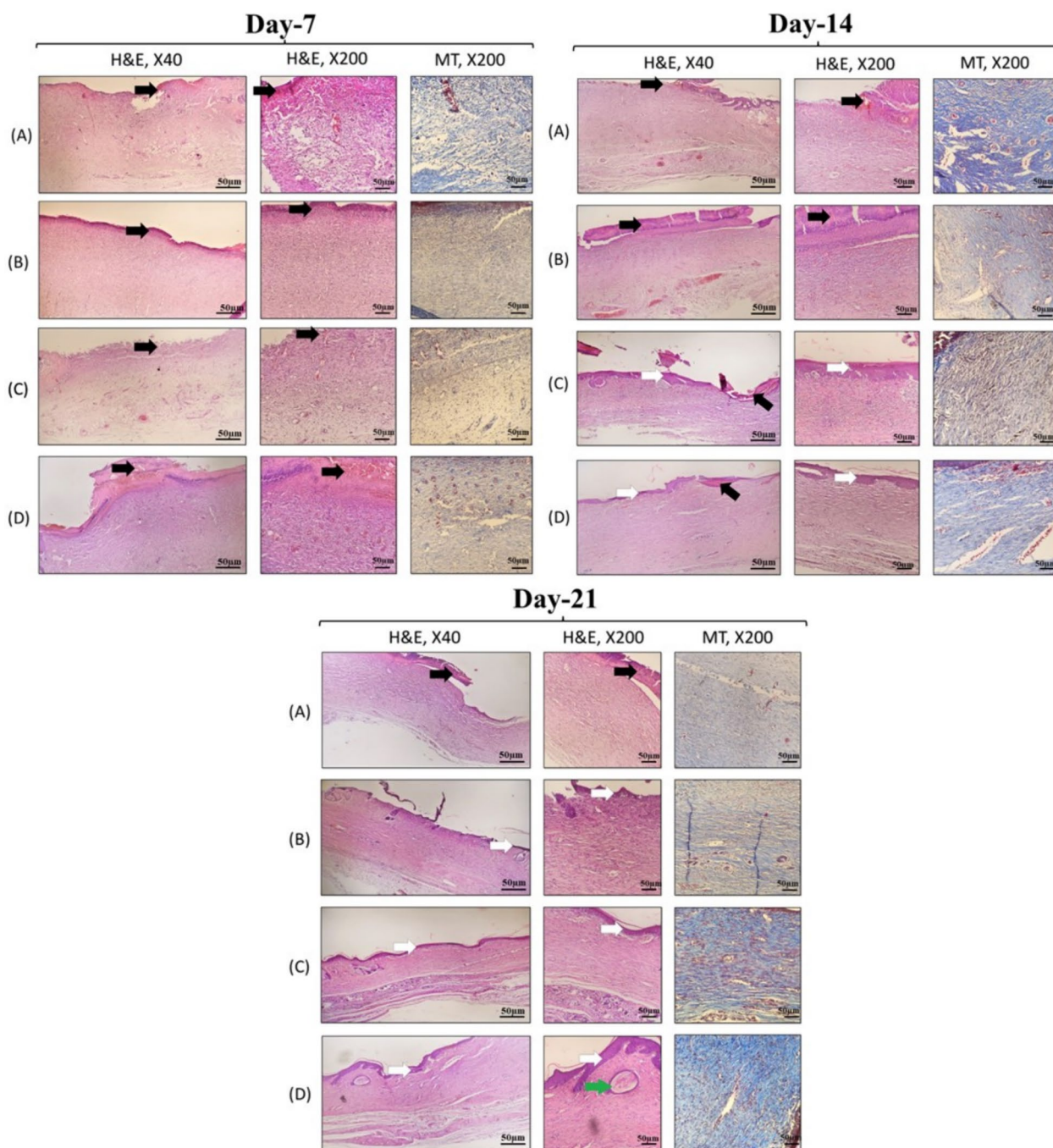


**Fig. 10** Histopathological results of the treated wound tissue that stained with H&E and MT in the diabetic rat at days 7, 14, and 21. **A** Untreated (control), **B** Scaffold (CS70), **C** ADMSC + Scaffold (CS70-A), and **D** PLMSC + Scaffold (CS70-P). Black arrows: crusty scab, white arrows: re-epithelialization, green arrows: rejuvenation of hair follicles (Scale bar: 50µm)

solution of the impaired healing process in the chronic wound but most of them address one of the complex issues of chronic wound environment. So it is necessary to develop a multifunctional patch that can address more unresolved issues of the wound environment.

Some limitations including inadequate mechanical properties, low flexibility, and elasticity cause wound dressings to show inadequate treatment in clinical trials [96, 97]. So development of nanofiber composite patch impregnated mesenchymal stem cells can be a

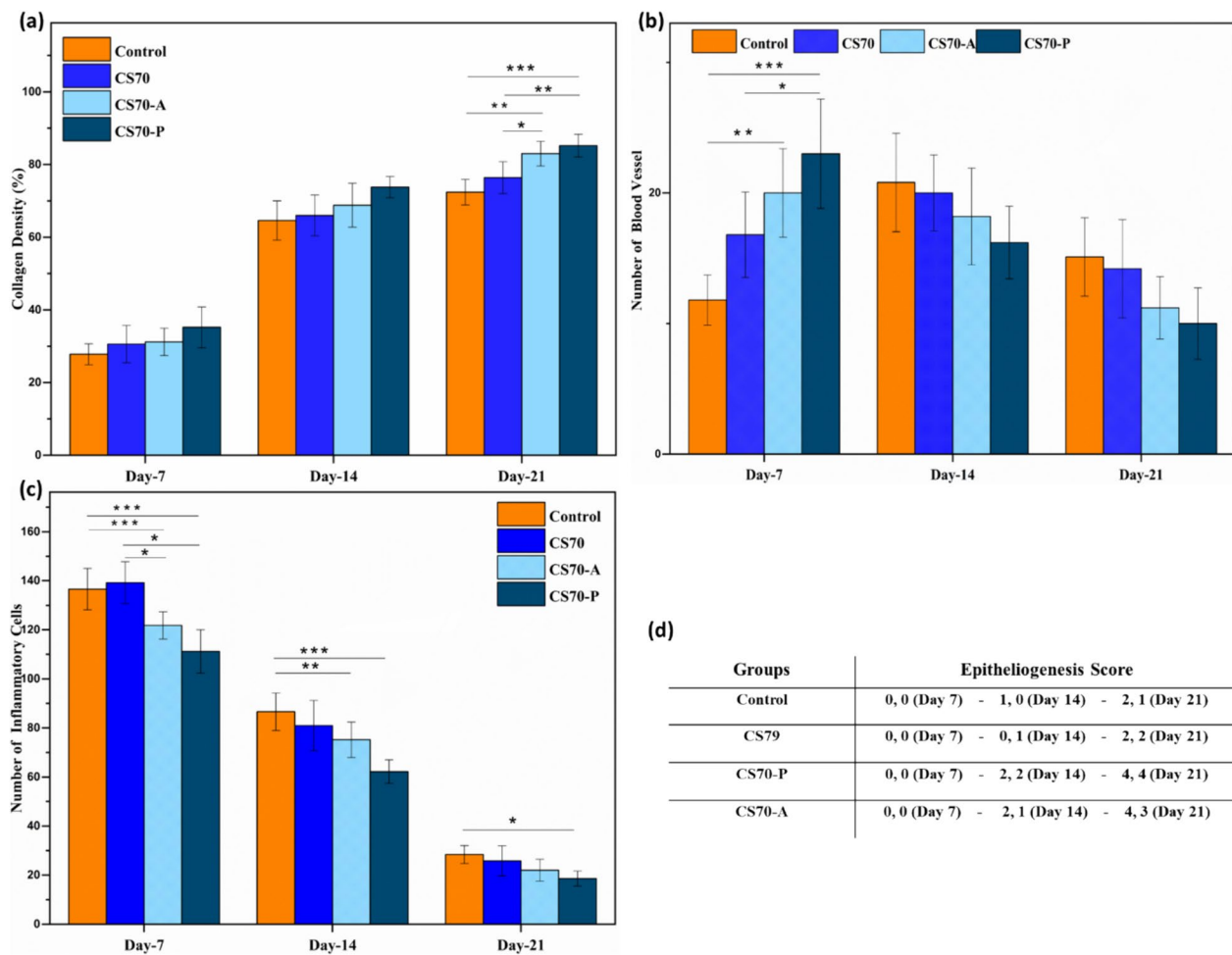


**Fig. 11** Representative graphs of collagen density, blood vessels, and inflammatory cells in wound sites of the different groups during the healing process. **a** Quantitative analysis of collagen density at days 7, 14, and 21 days, **b** Quantitative analysis of vascular density at days 7, 14, and 21 days, **c** Quantitative analysis of inflammatory cells at days 7, 14, and 21 days. (\* $p < 0.05$ , \*\* $p < 0.01$  and \*\*\* $p < 0.001$ ). **d** Histomorphometric analysis of different experimental groups

suitable solution for non-healing wounds. Due to (a) nanofiber structure having ECM-like architecture and other mentioned specific characters of nanofibers, (b) The presence of useful biopolymer in the structure of nano-scaffolds such as chitosan with well-known bacteriostatic properties and wound healing effects [98], (c) improved mechanical properties for better mimic of human skin, (d) paracrine effects of MSCs in the healing process, (e) the synergistic effect of nano scaffold with MSCs, our cellular nanofiber composite scaffold using a simplified nano extrusion technique as wound dressers can show valuable therapeutic effect for chronic wound treatment. SEM analysis confirmed nanofibrous morphology with a network of uniform nanofibers and narrow diameters (Fig. 1). According to biodegradation results, Chitosan, as the main polymer in the scaffold structure, was broken by the lysozyme

from the glycosidic bond. In addition, other polymers can be decomposed by this enzyme in the scaffold structure [99, 100]. The results of Fig. 3f and the normal skin's mechanical properties confirmed our fabricated scaffolds have appropriate mechanical properties for wound dressing applications. Also, this result shows tensile stress for the dry CS70 is lower compared to the CS80 which has a higher chitosan ratio, so it is the better choice because its tensile stress is closer to skin one [101]. Moreover, better swelling, more hydrophilicity, and higher biodegradation rate of CS70 persuaded us to continue our further investigations with this formulation. Development of the chitosan-based constructs for tissue engineering applications has some challenges in cell adhesion and proliferation, researchers investigated various strategies for improving their biological operation [102–106]. One of the popular methods for

enhancing cell adhesion and proliferation is surface modification [107–109]. That is why we used collagen type I coating as an efficient approach to improve cell behavior. The collagen-coated scaffolds were successfully seeded with MSCs (SEM and PI-DAPI staining). Based on the MTT assay, our nano bioscaffolds not only had no negative effect on cell proliferation but also could improve cell growth. It can be due to the presence of natural biodegradable polymers in composition, nanofibrous structure, and specific surface area. Also, the other results (Figures S3 and S4) confirmed MSCs attachment and proliferation on the scaffold after 5 days. Some studies indicated that Coating a surface with collagen can increase the tendency of cells to attach to the surface and proliferation [85, 110]. According to animal studies, cellular-treatment groups (CS70-P and CS70-A) showed notable healing compared to the control and acellular groups. As it is predicted after 21 days post-treatment according to many studies often complete wound healing is achieved by various wound dressings [111–113]. So the achievement of a faster wound closure rate in the earlier time points post-treatment can show better effectiveness of MSCs together with the nano scaffold. The paracrine effect of MSCs by secreting various growth factors can make up for the extensive loss of growth factors in the wound site and can increase the speed of the healing process and wound closure [114–117]. The CS70-P group showed the greatest similarity to normal skin at day 21 post-treatment, with skin appendage formation. Overall, the PLMSC-treated wounds showed the best histopathological results compared to other groups. As seen in Fig. 10, the collagen fibers in the CS70-P treatment group were denser, more regular, and parallel than other groups. The regular and dense pattern of collagen fibers in the wound area leads to a reduction in the possibility of scarring and contributes to the success of the treatment [118]. Also, detailed investigations in this field can be evaluated in future studies. As known in the first days post-injury in the wound healing process, inflammatory cells increase in the wound site and show helpful effects by secretion of proteases and phagocytosis of local bacteria and necrotic tissue during the first days (Fig. 11c). The prolonged presence could cause a defect in the healing process and delay treatment as seen in the diabetic wound bed. So the number of inflammatory cells often starts decreasing after 7 days post-treatment [119–121]. In summary, the results show that re-epithelialization in the MSCs treatment group was higher than in the two other groups. Furthermore, the PLMSC-scaffold group had the best re-epithelialization and was more like normal skin. Moreover, it should be mentioned, that further studies

are needed to explore the mechanism behind MSCs-scaffold interaction. It is worth mentioning that the immunogenicity of the scaffolds should be evaluated before clinical application but we did not assess it in our preliminary proof of concept study.

## Conclusion

To preliminarily study the synergistic effect of cellular nanofiber composite scaffold on chronic wounds, especially diabetic ones, we used a nano extrusion device to fabricate a nanoporous membrane with biodegradable polymers. PLMSCs and ADMSCs were loaded onto nano-bioscaffolds for delivery to the wound sites. To obtain the attachment of MSCs on the scaffolds, the collagen coating method was used. After various physicochemical analyses, the scaffold with superior properties was used for full-thickness diabetic wounds in the rat model. The results show cellular groups exhibited enhanced wound healing compared to control an acellular. Additionally, in cellular groups, CS70-P demonstrated better tissue regeneration. So PLMSC+nanofibrous CS70 scaffold showed superior therapeutic efficacy in chronic wound healing and skin regeneration. It is suggested that for clinical applications, more studies on the optimization of tissue-engineered grafts and safety need to be done.

## Limitation

This study as a preliminary study is a proof of concept. Our focus was preparing the cellular nano-bioscaffold that closely mimics the extracellular matrix to take advantage of the synergic effect of this combination. For more evaluation of MSCs' healing effect in vivo, it is better to evaluate the separated treatment groups including ADMSC and PLMSC injection and we will consider this in future studies. In the current experiment, we did not perform in vivo stability studies. We completely agree that a deeper stability study is essential before going to a clinical trial.

## Abbreviations

|         |  |              |
|---------|--|--------------|
| RM      | Regenerative medicine,                                     |              |
| MSC     | Mesenchymal stem cell                                      |              |
| ECM     | Extracellular matrix                                       |              |
| FBS     | Phosphate-buffered saline                                  |              |
| EB      | Epidermolysis Bullosa                                      |              |
| ADMSCs  | Human adipose-derived MSCs                                 |              |
| PLMSCs  | Placenta-derived MSCs                                      |              |
| DAPI    | 4',6-Diamidino-2-phenylindole                              |              |
| STZ     | Streptozotocin   |              |
| DMEM    | Dulbecco's modified eagle medium                           |              |
| PSR     | Picro-Sirius red   |              |
| EDC/NHS | 1-Ethyl-3-(3-dimethyl<br>carbodiimide/N-hydroxysuccinimide | aminopropyl) |
| DMSO    | Dimethylsulfoxide  |              |
| H&E     | Hematoxylin and eosin                                      |              |
| MT      | Masson's trichrome   |              |



## Supplementary Information

The online version contains supplementary material available at <https://doi.org/10.1186/s13287-024-03772-7>.

Supplementary file 1

### Acknowledgements

We are grateful to the pharmacy faculty at Tehran University Medical Science for financial support and for providing equipment.

### Author contributions

AA investigated, formulated, and fabricated samples, performed in vitro and in vivo experiments, collected and analyzed data, and wrote manuscripts. HRA managed in vitro experiments, data analyzed and critically revised the manuscript. ZM fabricated samples and analyzed data. HRM performed in vivo experiments and analyzed data. SM analyzed data. MA illustrated a graphical abstract. SNO revised the manuscript. BL revised the manuscript. MR investigated, organized, and managed experiments, analyzed data, and revised the manuscript. HAJ organized and supervised the study, analyzed the data, and critically revised the manuscript.

### Funding

This research was supported by the pharmaceutical research center of pharmacy faculty at Tehran University Medical Science (NO: 97-03-33-37930) and the Endocrinology and Metabolism Research Institute of Tehran University Medical Science.

### Availability of data and materials

All data in this research study are available from the corresponding author upon reasonable request.

### Declarations

#### Ethics approval and consent to participate

The project entitled: "Evaluation of the regenerative potential of mesenchymal stem cell in chitosan-based composite nano scaffold for diabetic wound healing" was approved by the ethics committee (IRB) of the Institute of Pharmaceutical Science, Tehran University of Medical Sciences, Tehran, Iran (Approval ID: IR.TUMS.TIPS.REC.1397.084, Approval Date: 2018-11-06). Placenta and adipose tissue donation were done after obtaining written informed consent from the donors. All Animal experiments were done according to the "Guideline for the Care and Use of Laboratory Animals in Iran" (<https://ethics.research.ac.ir/docs/pages/Guideline-En.pdf>).

#### Consent for publication

Not applicable.

#### Competing interests

The authors report no conflicts of interest in this work.

#### Author details

<sup>1</sup>Department of Pharmaceutical Biomaterials, Faculty of Pharmacy, Tehran University of Medical Sciences, Tehran, Iran. <sup>2</sup>Cell Therapy and Regenerative Medicine Research Center, Endocrinology and Metabolism Molecular-Cellular Sciences Institute, Tehran University of Medical Sciences, Tehran, Iran. <sup>3</sup>Faculty of Pharmacy, Tehran University of Medical Sciences, Tehran, Iran. <sup>4</sup>Dental Research Center, Dentistry Research Institute, Tehran University of Medical Sciences, Tehran, Iran. <sup>5</sup>Department of Pharmaceutical Nanotechnology, Faculty of Pharmacy, Tehran University of Medical Sciences, Tehran, Iran. <sup>6</sup>Department of Pharmaceutical Biotechnology, School of Pharmacy, Shahid Beheshti University of Medical Sciences, Tehran, Iran. <sup>7</sup>Department of Toxicology and Pharmacology, Faculty of Pharmacy, Tehran University of Medical Sciences, Tehran, Iran. <sup>8</sup>Endocrinology and Metabolism Research Center, Endocrinology and Metabolism Clinical Sciences Institute, Tehran University of Medical Sciences, Tehran, Iran. <sup>9</sup>Nanotechnology Research Center, Faculty of Pharmacy, Tehran University of Medical Sciences, Tehran 13169-43551, Iran. <sup>10</sup>Department of Pharmaceutics, Faculty of Pharmacy, Tehran University of Medical Sciences, Tehran, Iran.

Received: 17 January 2024 Accepted: 27 May 2024

Published online: 15 August 2024

### Reference s

- Aghayan HR, Hosseini MS, Gholami M, Mohamadi-Jahani F, Tayanloo-Beik A, Alavi-Moghadam S, et al. Mesenchymal stem cells' seeded amniotic membrane as a tissue-engineered dressing for wound healing. *Drug Deliv Transl Res*. 2022;12(3):538–49.
- Datta S, Rameshbabu AP, Bankoti K, Maity PP, Das D, Pal S, et al. Oleoyl-chitosan-based nanofiber mats impregnated with amniotic membrane derived stem cells for accelerated full-thickness excisional wound healing. *ACS Biomater Sci Eng*. 2017;3(8):1738–49.
- Chouhan D, Dey N, Bhardwaj N, Mandal BB. Emerging and innovative approaches for wound healing and skin regeneration: current status and advances. *Biomaterials*. 2019;216: 119267.
- Tottoli EM, Dorati R, Genta I, Chiesa E, Pisani S, Conti B. Skin Wound Healing Process and New Emerging Technologies for Skin Wound Care and Regeneration. *Pharmaceutics*. 2020;12(8).
- Miguel SP, Sequeira RS, Moreira AF, Cabral CSD, Mendonça AG, Ferreira P, et al. An overview of electrospun membranes loaded with bioactive molecules for improving the wound healing process. *Eur J Pharm Biopharm*. 2019;139:1–22.
- Ramachandran A, Snehalatha C, Shetty AS, Nanditha A. Trends in prevalence of diabetes in Asian countries. *World J Diabetes*. 2012;3(6):110–7.
- Shaw JE, Sicree RA, Zimmet PZ. Global estimates of the prevalence of diabetes for 2010 and 2030. *Diabetes Res Clin Pract*. 2010;87(1):4–14.
- Armstrong DG, Boulton AJM, Bus SA. Diabetic foot ulcers and their recurrence. *N Engl J Med*. 2017;376(24):2367–75.
- Armstrong DG, Wrobel J, Robbins JM. Guest editorial: are diabetes-related wounds and amputations worse than cancer? *Int Wound J*. 2007;4(4):286–7.
- Holl J, Kowalewski C, Zimek Z, Fiedor P, Kaminski A, Oldak T, et al. Chronic diabetic wounds and their treatment with skin substitutes. *Cells*. 2021;10(3).
- Gordon AJ, Alfonso AR, Nicholson J, Chiu ES. Evidence for healing diabetic foot ulcers with biologic skin substitutes: a systematic review and meta-analysis. *Ann Plast Surg*. 2019;83(4 Suppl):31–44.
- Vyas KS, Vasconez HC. Wound healing: biologics, skin substitutes. *Biomembranes Scaffolds Healthcare (Basel)*. 2014;2(3):356–400.
- Tavakoli S, Klar AS. Bioengineered skin substitutes: Advances and future trends. *Appl Sci*. 2021;11(4):1493.
- Du S, Zeugolis DI, O'Brien T. Scaffold-based delivery of mesenchymal stromal cells to diabetic wounds. *Stem Cell Res Ther*. 2022;13(1):426.
- Willerth SM, Sakiyama-Elbert SE. Combining stem cells and biomaterial scaffolds for constructing tissues and cell delivery. Cambridge, MA: StemBook; 2008.
- Chaudhari AA, Vig K, Baganizi DR, Sahu R, Dixit S, Dennis V, et al. Future prospects for scaffolding methods and biomaterials in skin tissue engineering: a review. *Int J Mol Sci*. 2016;17(12):1974.
- Vasita R, Katti DS. Nanofibers and their applications in tissue engineering. *Int J Nanomed*. 2006;1(1):15.
- Amani M, Rakhshani A, Maghsoudian S, Rasoulzadehzali M, Yoosefi S, Keihankhadiv S, et al. pH-sensitive bilayer electrospun nanofibers based on ethyl cellulose and Eudragit S-100 as a dual delivery system for treatment of the burn wounds; preparation, characterizations, and in-vitro/in-vivo assessment. *Int J Biol Macromol*. 2023;249: 126705.
- Lu T, Li Y, Chen T. Techniques for fabrication and construction of three-dimensional scaffolds for tissue engineering. *Int J Nanomedicine*. 2013;8:337–50.
- Mousivand Z, Ayazi H, Abdollahi A, Akbari H, Raoufi M, Sharifikolouei E. Hybrid electrospun scaffold loaded with Argireline acetate and Dexpanthenol for skin regeneration. *Int J Polym Mater Polym Biomater*. 2022;1–12.
- Raoufi M, Das T, Schoen I, Vogel V, Brüggemann D, Spatz JP. Nanopore diameters tune strain in extruded fibronectin fibers. *Nano Lett*. 2015;15(10):6357–64.
- Atashgah RB, Ghasemi A, Raoufi M, Abdollahifar MA, Zanganeh S, Nejadnik H, et al. Restoring endogenous repair mechanisms to heal



- chronic wounds with a multifunctional wound dressing. *Mol Pharm*. 2021;18(8):3171–80.
23. Matica MA, Aachmann FL, Tøndervik A, Sletta H, Ostafe V. Chitosan as a wound dressing starting material: antimicrobial properties and mode of action. *Int J Mol Sci*. 2019;20(23).
  24. Liu H, Wang C, Li C, Qin Y, Wang Z, Yang F, et al. A functional chitosan-based hydrogel as a wound dressing and drug delivery system in the treatment of wound healing. *RSC Adv*. 2018;8(14):7533–49.
  25. Abdollahi A, Malek-Khatibi A, Razavi MS, Sheikhi M, Abbaspour K, Rezaghali Z, et al. The recent advancement in the chitosan-based thermosensitive hydrogel for tissue regeneration. *J Drug Deliv Sci Technol*. 2023;104627.
  26. Litwiniuk M, Krejner A, Speyrer MS, Gauto AR, Grzela T. Hyaluronic acid in inflammation and tissue regeneration. *Wounds*. 2016;28(3):78–88.
  27. Mathew-Steiner SS, Roy S, Sen CK. Collagen in wound healing. *Bioengineering*. 2021;8(5):63.
  28. León-López A, Morales-Peñaloza A, Martínez-Juárez VM, Vargas-Torres A, Zeugolis DI, Aguirre-Álvarez G. Hydrolyzed collagen-sources and applications. *Molecules*. 2019;24(22).
  29. Bagheri Miyab K, Alipoor E, Vaghardoost R, Saberi Isfeedvajani M, Yaseri M, Djafarian K, et al. The effect of a hydrolyzed collagen-based supplement on wound healing in patients with burn: A randomized double-blind pilot clinical trial. *Burns*. 2020;46(1):156–63.
  30. Holmes C, Wrobel JS, Maceachern MP, Boles BR. Collagen-based wound dressings for the treatment of diabetes-related foot ulcers: a systematic review. *Diabetes Metab Syndr Obes*. 2013;6:17–29.
  31. Amirrah NI, Mohdrazipwee MF, Tabata Y, Bthjidrus R, Nordin A, Fauzi MB. Antibacterial-integrated collagen wound dressing for diabetes-related foot ulcers: An evidence-based review of clinical studies. *Polymers*. 2020;12(9):2168.
  32. Mbese Z, Alven S, Aderibigbe BA. Collagen-based nanofibers for skin regeneration and wound dressing applications. *Polymers*. 2021;13(24):4368.
  33. Golchin A, Farahany TZ, Khojasteh A, Soleimanifar F, Ardeshiryajimi A. The clinical trials of mesenchymal stem cell therapy in skin diseases: an update and concise review. *Curr Stem Cell Res Ther*. 2019;14(1):22–33.
  34. Huang YZ, Gou M, Da LC, Zhang WQ, Xie HQ. Mesenchymal stem cells for chronic wound healing: current status of preclinical and clinical studies. *Tissue Eng Part B Rev*. 2020;26(6):555–70.
  35. Zhang J, Qu X, Li J, Harada A, Hua Y, Yoshida N, et al. Tissue sheet engineered using human umbilical cord-derived mesenchymal stem cells improves diabetic wound healing. *Int J Mol Sci*. 2022;23(20).
  36. Kuhl T, Mezger M, Hausser I, Handgretinger R, Bruckner-Tuderman L, Nyström A. High local concentrations of intradermal MSCs restore skin integrity and facilitate wound healing in dystrophic epidermolysis bullosa. *Mol Ther*. 2015;23(8):1368–79.
  37. Petrova A, Georgiadis C, Fleck RA, Allison L, McGrath JA, Dazzi F, et al. Human mesenchymal stromal cells engineered to express collagen VII can restore anchoring fibrils in recessive dystrophic epidermolysis bullosa skin graft chimeras. *J Invest Dermatol*. 2020;140(1):121–31.e6.
  38. Riedl J, Popp C, Eide C, Ebens C, Tolar J. Mesenchymal stromal cells in wound healing applications: role of the secretome, targeted delivery and impact on recessive dystrophic epidermolysis bullosa treatment. *Cytotherapy*. 2021;23(11):961–73.
  39. Lee B-C, Kim J-J, Lee JY, Kang I, Shin N, Lee S-E, et al. Disease-specific primed human adult stem cells effectively ameliorate experimental atopic dermatitis in mice. *Theranostics*. 2019;9(12):3608.
  40. Park HH, Lee S, Yu Y, Yoo SM, Baek SY, Jung N, et al. TGF- $\beta$  secreted by human umbilical cord blood-derived mesenchymal stem cells ameliorates atopic dermatitis by inhibiting secretion of TNF- $\alpha$  and IgE. *Stem Cells*. 2020;38(7):904–16.
  41. Shin T-H, Lee B-C, Choi SW, Shin J-H, Kang I, Lee JY, et al. Human adipose tissue-derived mesenchymal stem cells alleviate atopic dermatitis via regulation of B lymphocyte maturation. *Oncotarget*. 2017;8(1):512.
  42. Sierra-Sánchez Á, Montero-Vilchez T, Quiñones-Vico MI, Sanchez-Diaz M, Arias-Santiago S. Current advanced therapies based on human mesenchymal stem cells for skin diseases. *Front Cell Dev Biol*. 2021;9:643125.
  43. Behm B, Babilas P, Landthaler M, Schreml S. Cytokines, chemokines and growth factors in wound healing. *J Eur Acad Dermatol Venereol*. 2012;26(7):812–20.
  44. Chen L, Tredget EE, Wu PY, Wu Y. Paracrine factors of mesenchymal stem cells recruit macrophages and endothelial lineage cells and enhance wound healing. *PLoS ONE*. 2008;3(4): e1886.
  45. Maxson S, Lopez EA, Yoo D, Danilkovitch-Miagkova A, Leroux MA. Concise review: role of mesenchymal stem cells in wound repair. *Stem Cells Transl Med*. 2012;1(2):142–9.
  46. Barba M, Di Taranto G, Lattanzi W. Adipose-derived stem cell therapies for bone regeneration. *Expert Opin Biol Ther*. 2017;17(6):677–89.
  47. Kong P, Xie X, Li F, Liu Y, Lu Y. Placenta mesenchymal stem cell accelerates wound healing by enhancing angiogenesis in diabetic Goto-Kakizaki (GK) rats. *Biochem Biophys Res Commun*. 2013;438(2):410–9.
  48. Ebrahimián TG, Pouzoulet F, Squiban C, Buard V, André M, Cousin B, et al. Cell therapy based on adipose tissue-derived stromal cells promotes physiological and pathological wound healing. *Arterioscler Thromb Vasc Biol*. 2009;29(4):503–10.
  49. Gu J, Liu N, Yang X, Feng Z, Qi F. Adipose-derived stem cells seeded on PLCL/P123 electrospun nanofibrous scaffold enhance wound healing. *Biomed Mater*. 2014;9(3): 035012.
  50. Álvaro-Afonso FJ, Sanz-Corbalaín I, Lázaro-Martínez JL, Kakagia D, Papanas N. Adipose-derived mesenchymal stem cells in the treatment of diabetic foot ulcers: a review of preclinical and clinical studies. *Angiology*. 2020;71(9):853–63.
  51. Luck J, Weil BD, Lowdell M, Mosahebi A. Adipose-derived stem cells for regenerative wound healing applications: understanding the clinical and regulatory environment. *Aesthet Surg J*. 2020;40(7):784–99.
  52. Zeng X, Tang Y, Hu K, Jiao W, Ying L, Zhu L, et al. Three-week topical treatment with placenta-derived mesenchymal stem cells hydrogel in a patient with diabetic foot ulcer: a case report. *Medicine (Baltimore)*. 2017;96(51): e9212.
  53. Meamar R, Ghasemi-Mobarakeh L, Norouzi MR, Siavash M, Hamblin MR, Fesharaki M. Improved wound healing of diabetic foot ulcers using human placenta-derived mesenchymal stem cells in gelatin electrospun nanofibrous scaffolds plus a platelet-rich plasma gel: a randomized clinical trial. *Int Immunopharmacol*. 2021;101(Pt B): 108282.
  54. Pelekanos RA, Sardesai VS. Human placenta-derived mesenchymal stem/stromal cells: fetal and maternal origins and critical parameters for ex vivo expansion. *Biol Therapeut Appl Mesenchymal Cells*. 2016:32–8.
  55. Marquardt LM, Heilshorn SC. Design of injectable materials to improve stem cell transplantation. *Curr Stem Cell Rep*. 2016;2(3):207–20.
  56. Willerth SM, Sakiyama-Elbert SE. Combining stem cells and biomaterial scaffolds for constructing tissues and cell delivery. *StemJournal*. 2019;1(1):1–25.
  57. Cosson S, Otte EA, Hezaveh H, Cooper-White JJ. Concise review: tailoring bioengineered scaffolds for stem cell applications in tissue engineering and regenerative medicine. *Stem Cells Transl Med*. 2015;4(2):156–64.
  58. Xu Y, Chen C, Hellwarth PB, Bao X. Biomaterials for stem cell engineering and biomanufacturing. *Bioactive Mater*. 2019;4:366–79.
  59. Krishna L, Dhamodaran K, Jayadev C, Chatterjee K, Shetty R, Khora SS, et al. Nanostructured scaffold as a determinant of stem cell fate. *Stem Cell Res Ther*. 2016;7(1):188.
  60. Andonegi M, Heras KL, Santos-Vizcaino E, Igartua M, Hernandez RM, de la Caba K, et al. Structure-properties relationship of chitosan/collagen films with potential for biomedical applications. *Carbohydr Polym*. 2020;237: 116159.
  61. Wang S, Zhao G. Quantitative characterization of the electrospun gelatin-chitosan nanofibers by coupling scanning electron microscopy and atomic force microscopy. *Mater Lett*. 2012;79:14–7.
  62. Taylor M, Urquhart AJ, Zelzer M, Davies MC, Alexander MR. Pico-liter water contact angle measurement on polymers. *Langmuir*. 2007;23(13):6875–8.
  63. Aguirre-Loredo RY, Rodríguez-Hernández AI, Morales-Sánchez E, Gómez-Aldapa CA, Velazquez G. Effect of equilibrium moisture content on barrier, mechanical and thermal properties of chitosan films. *Food Chem*. 2016;196:560–6.
  64. Wilgus TA, Roy S, McDaniel JC. Neutrophils and wound repair: positive actions and negative reactions. *Adv Wound Care (New Rochelle)*. 2013;2(7):379–88.
  65. Aghayan HR, Payab M, Mohamadi-Jahani F, Aghayan SS, Larjani B, Arjmand B. GMP-compliant production of human placenta-derived mesenchymal stem cells. *Methods Mol Biol*. 2021;2286:213–25.

66. Aghayan HR, Goodarzi P, Arjmand B. GMP-compliant human adipose tissue-derived mesenchymal stem cells for cellular therapy. *Methods Mol Biol.* 2015;1283:93–107.
67. Menon AH, Soundarya SP, Sanjay V, Chandran SV, Balangadharan K, Selvamurugan N. Sustained release of chrysin from chitosan-based scaffolds promotes mesenchymal stem cell proliferation and osteoblast differentiation. *Carbohydr Polym.* 2018;195:356–67.
68. Sharif S, Ai J, Azami M, Verdi J, Atlasi MA, Shirian S, et al. Collagen-coated nano-electrospun PCL seeded with human endometrial stem cells for skin tissue engineering applications. *J Biomed Mater Res B Appl Biomater.* 2018;106(4):1578–86.
69. Ao H, Xie Y, Tan H, Wu X, Liu G, Qin A, et al. Improved hMSC functions on titanium coatings by type I collagen immobilization. *J Biomed Mater Res A.* 2014;102(1):204–14.
70. Delaine-Smith RM, MacNeil S, Reilly GC. Matrix production and collagen structure are enhanced in two types of osteogenic progenitor cells by a simple fluid shear stress stimulus. *Eur Cell Mater.* 2012;24:162–74.
71. Diaz-Gomez L, Alvarez-Lorenzo C, Concheiro A, Silva M, Dominguez F, Sheikh FA, et al. Biodegradable electrospun nanofibers coated with platelet-rich plasma for cell adhesion and proliferation. *Mater Sci Eng, C.* 2014;40:180–8.
72. Tolosa L, Donato MT, Gómez-Lechón MJ. General cytotoxicity assessment by means of the MTT assay. *Methods Mol Biol.* 2015;1250:333–48.
73. Furman BL. Streptozotocin-induced diabetic models in mice and rats. *Curr Protocols Pharmacol.* 2015;70(1):5–47.
74. Wang X, Ge J, Tredget EE, Wu Y. The mouse excisional wound splinting model, including applications for stem cell transplantation. *Nat Protoc.* 2013;8(2):302–9.
75. Kim UJ, Park J, Kim HJ, Wada M, Kaplan DL. Three-dimensional aqueous-derived biomaterial scaffolds from silk fibroin. *Biomaterials.* 2005;26(15):2775–85.
76. Ma L, Gao C, Mao Z, Zhou J, Shen J, Hu X, et al. Collagen/chitosan porous scaffolds with improved biostability for skin tissue engineering. *Biomaterials.* 2003;24(26):4833–41.
77. Lončarević A, Ivanković M, Rogina A. Lysozyme-induced degradation of chitosan: the characterisation of degraded chitosan scaffolds. *J Tissue Repair Regen.* 2017;1:12–22.
78. Matica A, Menghiu G, Ostafe V. Biodegradability of chitosan based products. *New Front Chem.* 2017;26(1).
79. Kurita K, Kaji Y, Mori T, Nishiyama Y. Enzymatic degradation of  $\beta$ -chitin: susceptibility and the influence of deacetylation. *Carbohydr Polym.* 2000;42(1):19–21.
80. Huang J, Qin J, Zhang P, Chen X, You X, Zhang F, et al. Facile preparation of a strong chitosan-silk biocomposite film. *Carbohydr Polym.* 2020;229:115515.
81. Cai S, Wu C, Yang W, Liang W, Yu H, Liu L. Recent advance in surface modification for regulating cell adhesion and behaviors. *Nanotechnol Rev.* 2020;9(1):971–89.
82. Kukumberg M, Yao Y, Goh SH, Neo DJ, Yao JY, Yim EK. Evaluation of the topographical influence on the cellular behavior of human umbilical vein endothelial cells. *Adv Biosyst.* 2018;2(6):1700217.
83. Langhe RP, Gudzenko T, Bachmann M, Becker SF, Gonnermann C, Winter C, et al. Cadherin-11 localizes to focal adhesions and promotes cell–substrate adhesion. *Nat Commun.* 2016;7(1):10909.
84. Maghdouri-White Y, Bowlin GL, Lemmon CA, Dréau D. Mammary epithelial cell adhesion, viability, and infiltration on blended or coated silk fibroin-collagen type I electrospun scaffolds. *Mater Sci Eng C Mater Biol Appl.* 2014;43:37–44.
85. He W, Yong T, Teo WE, Ma Z, Ramakrishna S. Fabrication and endothelialization of collagen-blended biodegradable polymer nanofibers: potential vascular graft for blood vessel tissue engineering. *Tissue Eng.* 2005;11(9–10):1574–88.
86. Rich L, Whittaker P. Collagen and picrosirius red staining: a polarized light assessment of fibrillar hue and spatial distribution. *J Morphol Sci* 2017;22(2):0-.
87. Lattouf R, Younes R, Lutowski D, Naaman N, Godeau G, Senni K, et al. Picrosirius red staining: a useful tool to appraise collagen networks in normal and pathological tissues. *J Histochem Cytochem.* 2014;62(10):751–8.
88. Lee MH, You C, Kim KH. Combined effect of a microporous layer and Type I collagen coating on a biphasic calcium phosphate scaffold for bone tissue engineering. *Materials (Basel).* 2015;8(3):1150–61.
89. Motasadzadeh H, Tavakoli M, Damoogh S, Mottaghitalab F, Gholami M, Atyabi F, et al. Dual drug delivery system of teicoplanin and phenamil based on pH-sensitive silk fibroin/sodium alginate hydrogel scaffold for treating chronic bone infection. *Biomater Adv.* 2022;139: 213032.
90. Li M, Chen J, Shi M, Zhang H, Ma PX, Guo B. Electroactive anti-oxidant polyurethane elastomers with shape memory property as non-adherent wound dressing to enhance wound healing. *Chem Eng J.* 2019;375: 121999.
91. Feng X, Zhang X, Li S, Zheng Y, Shi X, Li F, et al. Preparation of aminated fish scale collagen and oxidized sodium alginate hybrid hydrogel for enhanced full-thickness wound healing. *Int J Biol Macromol.* 2020;164:626–37.
92. Zhou X, Wang H, Zhang J, Li X, Wu Y, Wei Y, et al. Functional poly ( $\epsilon$ -caprolactone)/chitosan dressings with nitric oxide-releasing property improve wound healing. *Acta Biomater.* 2017;54:128–37.
93. Lin Z, Wu T, Wang W, Li B, Wang M, Chen L, et al. Biofunctions of antimicrobial peptide-conjugated alginate/hyaluronic acid/collagen wound dressings promote wound healing of a mixed-bacteria-infected wound. *Int J Biol Macromol.* 2019;140:330–42.
94. Nunan R, Harding KG, Martin P. Clinical challenges of chronic wounds: searching for an optimal animal model to recapitulate their complexity. *Dis Model Mech.* 2014;7(11):1205–13.
95. Eming SA, Martin P, Tomic-Canic M. Wound repair and regeneration: mechanisms, signaling, and translation. *Sci Transl Med.* 2014;6(265):265.
96. Dreifke MB, Jayasuriya AA, Jayasuriya AC. Current wound healing procedures and potential care. *Mater Sci Eng, C.* 2015;48:651–62.
97. Zhong S, Zhang Y, Lim C. Tissue scaffolds for skin wound healing and dermal reconstruction. *Wiley Interdiscipl Rev Nanomed Nanobiotechnol.* 2010;2(5):510–25.
98. Jayakumar R, Prabaharan M, Kumar PS, Nair S, Tamura H. Biomaterials based on chitin and chitosan in wound dressing applications. *Biotechnol Adv.* 2011;29(3):322–37.
99. Wang HM, Chou YT, Wen ZH, Wang CZ, Chen CH, Ho ML. Novel biodegradable porous scaffold applied to skin regeneration. *PLoS ONE.* 2013;8(6): e56330.
100. Shah R, Stodulka P, Skopalova K, Saha P. Dual crosslinked collagen/chitosan film for potential biomedical applications. *Polymers (Basel).* 2019;11(12).
101. Hussain SH, Limthongkul B, Humphreys TR. The biomechanical properties of the skin. *Dermatol Surg.* 2013;39(2):193–203.
102. Custódio CA, Alves CM, Reis RL, Mano JF. Immobilization of fibronectin in chitosan substrates improves cell adhesion and proliferation. *J Tissue Eng Regen Med.* 2010;4(4):316–23.
103. Ruprai H, Romanazzo S, Ireland J, Kilian K, Mawad D, George L, et al. Porous chitosan films support stem cells and facilitate sutureless tissue repair. *ACS Appl Mater Interfaces.* 2019;11(36):32613–22.
104. Aljawish A, Muniglia L, Chevalot I. Growth of human mesenchymal stem cells (MSCs) on films of enzymatically modified chitosan. *Biotechnol Prog.* 2016;32(2):491–500.
105. Zhuang PY, Li YL, Fan L, Lin J, Hu QL. Modification of chitosan membrane with poly(vinyl alcohol) and biocompatibility evaluation. *Int J Biol Macromol.* 2012;50(3):658–63.
106. Sun M, Yuan L, Yang X, Shao L. Preparation and modification of chitosan-based membrane. *ES Mater Manuf.* 2020;9(2):40–7.
107. Luna SM, Silva SS, Gomes ME, Mano JF, Reis RL. Cell adhesion and proliferation onto chitosan-based membranes treated by plasma surface modification. *J Biomater Appl.* 2011;26(1):101–16.
108. Park BU, Park SM, Lee KP, Lee SJ, Nam YE, Park HS, et al. Collagen immobilization on ultra-thin nanofiber membrane to promote in vitro endothelial monolayer formation. *J Tissue Eng.* 2019;10:2041731419887833.
109. Amani H, Arzaghi H, Bayandori M, Dezfuli AS, Pazoki-Toroudi H, Shafiee A, et al. Controlling cell behavior through the design of biomaterial surfaces: a focus on surface modification techniques. *Adv Mater Interfaces.* 2019;6(13):1900572.
110. He W, Ma Z, Yong T, Teo WE, Ramakrishna S. Fabrication of collagen-coated biodegradable polymer nanofiber mesh and its potential for endothelial cells growth. *Biomaterials.* 2005;26(36):7606–15.

111. Yu H, Chen X, Cai J, Ye D, Wu Y, Fan L, et al. Novel porous three-dimensional nanofibrous scaffolds for accelerating wound healing. *Chem Eng J*. 2019;369:253–62.
112. Wu Y-Y, Jiao Y-P, Xiao L-L, Li M-M, Liu H-W, Li S-H, et al. Experimental study on effects of adipose-derived stem cell-seeded silk fibroin chitosan film on wound healing of a diabetic rat model. *Ann Plast Surg*. 2018;80(5):572.
113. Rezvanian M, Ng SF, Alavi T, Ahmad W. In-vivo evaluation of Alginate-Pectin hydrogel film loaded with Simvastatin for diabetic wound healing in Streptozotocin-induced diabetic rats. *Int J Biol Macromol*. 2021;171:308–19.
114. Bruna F, Contador D, Conget P, Erranz B, Sossa CL, Arango-Rodríguez ML. Regenerative potential of mesenchymal stromal cells: age-related changes. *Stem Cells Int*. 2016;2016.
115. Gu C, Huang S, Gao D, Wu Y, Li J, Ma K, et al. Angiogenic effect of mesenchymal stem cells as a therapeutic target for enhancing diabetic wound healing. *Int J Low Extrem Wounds*. 2014;13(2):88–93.
116. Kuo Y-R, Wang C-T, Cheng J-T, Kao G-S, Chiang Y-C, Wang C-J. Adipose-derived stem cells accelerate diabetic wound healing through the induction of autocrine and paracrine effects. *Cell Transplant*. 2016;25(1):71–81.
117. Ariyanti AD, Zhang J, Marcelina O, Nugrahaningrum DA, Wang G, Kasim V, et al. Salidroside-pretreated mesenchymal stem cells enhance diabetic wound healing by promoting paracrine function and survival of mesenchymal stem cells under hyperglycemia. *Stem Cells Transl Med*. 2019;8(4):404–14.
118. Kim YS, Lew DH, Tark KC, Rah DK, Hong JP. Effect of recombinant human epidermal growth factor against cutaneous scar formation in murine full-thickness wound healing. *J Korean Med Sci*. 2010;25(4):589–96.
119. Kouhbananejad SM, Derakhshani A, Vahidi R, Dabiri S, Fatemi A, Armin F, et al. A fibrinous and allogeneic fibroblast-enriched membrane as a biocompatible material can improve diabetic wound healing. *Biomater Sci*. 2019;7(5):1949–61.
120. Reinke J, Sorg H. Wound repair and regeneration. *Eur Surg Res*. 2012;49(1):35–43.
121. Heublein H, Bader A, Giri S. Preclinical and clinical evidence for stem cell therapies as treatment for diabetic wounds. *Drug Discovery Today*. 2015;20(6):703–17.

### Publisher's Note

Springer Nature remains neutral with regard to jurisdictional claims in published maps and institutional affiliations.